Biochemical Pharmacology 246 (2026) 117707

Contents lists available at ScienceDirect

Biochemical Pharmacology

journal homepage: www.elsevier.com/locate/biochempharm

LIFR antagonism reverses epithelial pro-CAF programs in pancreatic ductal adenocarcinoma

Cristina Di Giorgio [a,*], Maria Rosaria Sette [a], Benedetta Sensini [a], Eleonora Giannelli [a], Ginevra Lachi [a], Silvia Marchianò [a], Francesca Paniconi [a], Carmen Massa [a], Ginevra Urbani [a], Rosa De Gregorio [b], Valentina Sepe [b], Maria Chiara Monti [b], Federica Moraca [b], Bruno Catalanotti [b], Fabio Cartaginese [d], Eleonora Distrutti [c], Angela Zampella [b], Michele Biagioli [a], Stefano Fiorucci [a,*]

[a] University of Perugia, Department of Medicine and Surgery, Perugia, Italy
[b] University of Naples Federico II, Department of Pharmacy, Naples, Italy
[c] Azienda Ospedaliera di Perugia, Perugia, Italy
[d] Azienda USL Umbria 1 - UOC Aziendale Anatomia Patologica Presidio Ospedaliero Alto Tevere - Ospedale di Città di Castello (PG), Italy

ARTICLE INFO

Keywords:
Pancreatic ductal adenocarcinoma
LIF/LIFR signalling
Cancer-associated fibroblasts
Stromal activation
JAK/STAT3
Desmoplasia
LIFR antagonists

ABSTRACT

Extracellular matrix remodelling that occurs in pancreatic ductal adenocarcinoma (PDAC) is considered a promoting factor of cancer growth, immune evasion and therapeutic resistance. Cancer-associated fibroblasts (CAFs) that constitute the dominant stromal population, arise primarily from activated pancreatic stellate cells and display remarkable functional heterogeneity, encompassing inflammatory iCAFs and contractile myCAFs. Although epithelial-stromal communication is central to PDAC biology, the upstream mechanisms that prime tumour cells toward CAF-Activating cells remain incompletely defined. The leukaemia inhibitory factor (LIF), a pleiotropic cytokine of the IL-6 family, is highly expressed in PDAC and has been implicated in tumour progression. However, the role of LIF and LIF receptor (LIFR):gp130 complex in promoting CAF activation is poorly defined. Here, we combined human PDAC transcriptomics, immunofluorescence and epithelial-stromal co-culture assays to define LIF-driven pro-CAF programs and evaluate their pharmacological reversibility. In PDAC cancer cells, MIAPaCa-2 cells, LIF induced a coordinated transcriptional network encompassing inflammatory mediators, paracrine fibroblast-activating signals and ECM/mechanotransductive modules, while repressing stromal-inhibitory genes. These signatures were recapitulated in PDAC tissues, where LIF expression directly correlated with CAF markers and with stromal remodelling genes. On this background, we have developed a novel steroidal LIFR antagonist, LRI310, and evaluate its effects on LIF:LIFR axis. Exposure of PDCA cell lines to LRI310 suppresses STAT3 activation and counteracts effects of LIF on proliferation and CAF-inducing transcriptional programs. Collectively, these findings identify LIF as an important epithelial driver of CAF-oriented transcriptional programs in PDAC and support the development of LIFR antagonism as a promising strategy to modulate the desmoplastic microenvironment.

Abbreviations: α-SMA, alpha-smooth muscle actin; ANOVA, analysis of variance; CAF, cancer-associated fibroblast; DEG, differentially expressed gene; DMSO, dimethyl sulfoxide; ECM, extracellular matrix; EMT, epithelial–mesenchymal transition; FBS, fetal bovine serum; gp130, glycoprotein 130; IC_{50}, half maximal inhibitory concentration; IF, immunofluorescence; IFNγ, interferon gamma; iCAF, inflammatory cancer-associated fibroblast; JAK, Janus kinase; LIF, leukemia inhibitory factor; LIFR, leukemia inhibitory factor receptor; myCAF, myofibroblastic cancer-associated fibroblast; OSM, oncostatin M; PBS, phosphate-buffered saline; PCA, principal component analysis; PDAC, pancreatic ductal adenocarcinoma; qPCR, quantitative polymerase chain reaction; RNA-seq, RNA sequencing; STAT3, signal transducer and activator of transcription 3.

* Corresponding authorsat: University of Perugia, Department of Medicine and Surgery, Section of Gastroenterology, Piazza L. Severi 1 – Edificio B, 06134 Perugia, Italy.

E-mail addresses: Cristina.digiorgio@studenti.unipg.it (C.D. Giorgio), Stefano.fiorucci@unipg.it (S. Fiorucci).

https://doi.org/10.1016/j.bcp.2026.117707
Received 1 December 2025; Received in revised form 9 January 2026; Accepted 12 January 2026
Available online 14 January 2026

1. Introduction

Pancreatic ductal adenocarcinoma (PDAC) is among the most lethal malignancies worldwide and is projected to become the second leading cause of cancer-related mortality within the next decade [1]. Its aggressive biology, early metastatic dissemination and limited responsiveness to chemotherapy continue to frustrate clinical management, but a defining hallmark of PDAC is its extensive desmoplastic reaction, which often constitutes more than 80% of the tumour mass [2]. This fibrotic stroma is composed of extracellular matrix (ECM), immune cells, vasculature and, most prominently, cancer-associated fibroblasts (CAFs), that strongly influence tumour growth while promote immune exclusion, metastatic potential and therapeutic resistance. Rather than serving as a structural bystander, the stromal cells act as a dynamic component of PDAC biology, shaping nutrient availability, tissue stiffness, drug penetration and inflammatory signalling [3,4].

CAFs originate largely from pancreatic stellate cells that, upon activation, acquire a myofibroblastic phenotype signed by expression of α-smooth muscle actin (α-SMA) and fibroblast activation proteins [5]. PDCA associated myofibroblasts display striking functional heterogeneity, encompassing contractile myCAFs, inflammatory iCAFs and antigen-presenting subsets, each regulated by distinct cytokines/chemokines within the tumour microenvironment [6–8]. Increasing evidence indicates that CAF contribute actively to PDAC progression by secreting ECM-remodelling proteins, cytokines, chemokines, growth factors and metabolites, thereby reinforcing tumour cell survival and therapeutic resistance [8]. However, despite their centrality, the upstream epithelial-derived signals that initiate and sustain CAF activation remain incompletely defined.

The Leukaemia Inhibitory Factor (LIF) is an IL-6 related cytokine that promotes PDAC aggressiveness. LIF signals through a heterodimeric receptor complex composed of LIFR and gp130, engaging JAK/STAT3, MAPK and PI3K/AKT cascades that orchestrate proliferation, stemness, EMT and chemoresistance in PDAC [7]. Elevated LIF expression is enriched in cancer tissues [9]. There is evidence that LIF/LIFR overexpression in PADC patients correlates with poor prognosis, KRAS-mutation and maintenance of tumour-initiating cells [10,11]. Importantly, both tumour cells and activated fibroblasts have been identified as sources of LIF within the PDAC microenvironment, suggesting that LIF may serve as a key mediator of epithelial-stromal reciprocity [12].

While LIF is known to drive tumour cell proliferation and STAT3 activation [13], its ability to reprogram epithelial cells toward the secretion of CAF-activating signals remains underexplored. Even less is known about the specific stromal genes and signalling modules induced downstream of LIF in human PDAC, particularly those related to ECM deposition, mechano-transduction, inflammatory signalling and suppression of stromal restraining pathways. The identification, of LIF-responsive stromal genes, could be of translational relevance, as they may represent previously unrecognized drivers of desmoplasia and chemotherapy resistance in LIF-high PDAC. Moreover, although protein-based LIF inhibitors have shown promise in preclinical models, small-molecule antagonists targeting LIFR remain scarce and no agents have entered clinical practice [14].

In this study, we sought to delineate the transcriptional programs activated by LIF in pancreatic cancer cells with particular focus on genes known to orchestrate fibroblast activation and stromal remodelling. By integrating RNA sequencing, human PDAC transcriptomics, histologic mapping and epithelial-stromal co-culture models, we aimed to uncover previously uncharacterized LIF-responsive genes that may function as pro-fibrotic stromal drivers in PDAC. In parallel, we evaluated the capacity of LRI310, a newly synthesized steroid-derived LIFR antagonist, to disrupt LIF/LIFR binding and attenuate LIF-dependent epithelial and stromal activation. Through this combined approach, we sought to clarify the role of LIF in shaping CAF biology and to explore the potential of LIFR inhibition as a strategy to counteract desmoplasia and its tumour-promoting consequences.

2. Material and methods

2.1. Cell cultures

2.1.1. Human pancreatic epithelial cells (MIAPACA 2)

MIAPACA2 cells were from ATCC (ATCC, Manassas, VA, USA). They were cultured in D-MEM high glucose medium (Euroclone, reference: ECB7501L) and supplemented with 10% of FBS, 1% L-Glutamine, and 1% of penicillin/streptomycin. For all experiments, cells were plated on Day 0 at the densities specified for each assay, allowed to adhere for 24 h, and subjected to serum starvation for an additional 24 h before treatment. When indicated, cells were exposed to recombinant LIF (10 ng/mL) alone or in combination with the LIFR antagonist LRI-310 at the concentrations detailed below.

2.1.2. Human liver epithelial cells (HEPG2)

HEPG2 cells (ATCC, Manassas, VA, USA) were maintained in Minimal Essential Medium (MEM, Euroclone Cat. No. ECB2071L) containing 10 % fetal bovine serum (FBS, Euroclone, Cat. No. ECS5000L), 1% L-glutamine (Euroclone, Cat. No. ECB3000D), and 1% penicillin–streptomycin solution (Euroclone, Cat. No. ECB30001D).

2.1.3. Human pancreatic stellate cells (HPanSteC)

HPanSteC cell line was provided from Innoprot and cultured in Stellate Cell Medium (Cat. No. P60126). The components of stellate cell medium kit were 500 mL of Basal Medium, 10 mL of fetal bovine serum, 5 mL of Stellate Cell Growth Supplement (SteCGS), and 5 mL of penicillin/stremtomycin solution (P/S solution).

2.1.4. RNA extraction

Total RNA was isolated from cultured cells using Tri-Reagent (Zymo Research) in combination with the Direct-zol™ RNA MiniPrep Kit with Zymo-Spin™ IIC Columns (Zymo Research, Irvine, CA). Genomic DNA contamination was removed by treatment with DNase I (Thermo Fisher Scientific, Waltham, MA). The purified RNA was subsequently employed for gene expression studies, including RNA sequencing and quantitative PCR (qPCR).

2.1.5. AmpliSeq transcriptome

RNA sequencing was performed on MIA PaCa-2 cells exposed to 10 ng/mL of recombinant LIF for 24 h or left untreated (NT). RNA concentration and integrity were evaluated with the Qubit® RNA HS Assay Kit on a Qubit 3.0 fluorometer and further verified by agarose gel electrophoresis.

Transcriptome libraries were prepared with the Ion AmpliSeq™ Transcriptome Human Gene Expression Core Panel in combination with the Chef-Ready Kit (Thermo Fisher Scientific). In brief, 10 ng of purified RNA were reverse-transcribed using the SuperScript™ Vilo™ cDNA Synthesis Kit. Library construction and barcoding were subsequently carried out on the Ion Chef™ system employing the Ion Code™ PCR Plate and the AmpliSeq™ Transcriptome panel, according to the manufacturer's instructions. Individual barcoded libraries were then pooled to a final concentration of 100 pM and used to generate Template-Positive Ion Sphere™ Particles with the Ion 540™ Kit-Chef. The prepared particles were loaded onto Ion 540™ Chips and sequenced on an Ion S5™ instrument using Torrent Suite™ Software v6. Differential gene expression analysis was performed with the Transcriptome Analysis Console (TAC) Software v4.0.2, applying thresholds of fold change < -2 or $> +2$ and a p-value < 0.05, as recommended for AmpliSeq datasets. The resulting transcriptomic dataset has been deposited in the Mendeley Data repository (https://doi.org/10.17632/sj3xhvmz44.1).

2.2. Human PDAC samples-internal cohort

Immunofluorescence staining of αSMA/LIF and LIFR was performed on liver biopsies obtained from patients with Pancreatic

Adenocarcinoma (n = 3). Study was conducted in accordance with institutional guidelines and approved under permission no. 357803.

2.3. GSE196009 data sets

The GSE196009 dataset (https://www.ncbi.nlm.nih.gov/geo/query/acc.cgi?acc=GSE196009), accessed on 1 August 2022, contains RNA-seq–based gene expression profiles generated using the Illumina HiSeq 2000 platform. The series includes fresh or cryo-preserved pancreatic ductal adenocarcinoma (PDAC) samples alongside matched non-tumorous pancreatic tissues collected from a cohort of 12 Japanese patients.

2.4. Histological analysis

2.4.1. Hematoxylin and Eosin (H/E)

For histopathological evaluation, human pancreas biopsies were collected, fixed in 10% neutral buffered formalin, embedded in paraffin, sectioned, and stained with hematoxylin and eosin (H&E) for morphometric evaluation.

2.4.2. Immunofluorescence (IF)

Immunofluorescence analyses were performed on paraffin-embedded human pancreas biopsy specimens and cultured cells (MIA PaCa-2 a human pancreatic cancer cell or human pancreatic stellate cells). Tissue sections were rehydrated and subjected to heat-induced antigen retrieval in sodium citrate buffer (pH 6.0) at 95 °C for 90 min, followed by cooling to room temperature for 30 min. After sequential washing (three times in distilled water and once in PBS), samples were incubated for 1 h at room temperature in blocking buffer (1 × PBS supplemented with 10% horse serum and 1% BSA).

Primary antibodies (see Table 1), diluted in blocking buffer, were applied to the samples and incubated overnight at 4 °C. The following day, sections were washed with PBS containing 0.1% Tween 20 (PBST) and subsequently incubated for 1 h at room temperature in the dark with the appropriate fluorophore-conjugated secondary antibodies (see Table 2). Autofluorescence was quenched with Sudan Black for 10 min, and nuclei were counterstained with DAPI for 1 min. Finally, slides were mounted using ProLong™ Glass Antifade Mountant, sealed, and imaged using an Olympus BX60 fluorescence microscope.

For in vitro experiments, cells (either untreated or stimulated with LIF, 10 ng/mL) were seeded onto chamber slides. At the indicated time points, cells were fixed in methanol for 20 min and processed according to the same immunofluorescence protocol, with omission of the Sudan Black quenching step.

Table 1
Primary antibody

Target	Antibody Details	Dilution	Supplier (Location)	Lot number	Secondary antibody used
Ki67	Mouse, Rat, Human	1:100	ABCAM	ab16667	Red
Vimentin	Mouse, Rat, Human, African green monkey	1:100	ABCAM	ab92547	Green
LIF	Human	1:100	INVITROGEN	PA5-79600	Red
LIFR	Human	1:100	ABCAM	ab235908	Green
αSMA	Human, Mouse, Rat	1:100	INVITROGEN eBIOSCIENCE	14–9760-82	Green

Table 2
Secondary antibody

Target	Light emitted	Dilution	Supplier (Location)	Lot number
Goat-Anti-Rabbit 568	Red	1:1000	INVITROGEN	a11011
Goat-Anti-Mouse 488	Green	1:200	INVITROGEN	a32723
Goat-Anti-Rabbit 488	Green	1:200	ABCAM	ab150077

2.4.3. Fluorescence quantification

Ki67 and Vimentin fluorescence signals in MIA PaCa-2 immunofluorescence images were quantified following the "Measuring Cell Fluorescence Using ImageJ" protocol (https://sciencetechblog.files.wordpress.com/2011/05/measuring-cell-fluorescence-using-imagej.pdf), which enables calculation of the corrected total cell fluorescence (CTCF).

2.4.4. Synthesis

The compound LRI310 was synthesized according to previously reported procedures [15].

2.4.5. AlphaScreen

Recombinant human LIFR (His-tagged) and biotinylated human LIF were obtained from Sino Biological (Düsseldorf, Germany) and R&D Systems (Abingdon, UK), respectively, and reconstituted following the manufacturers' instructions. The ability of LRI-310 to interfere with LIF–LIFR interaction was assessed using an AlphaScreen proximity assay. Reactions were performed in white, low-volume 384-well AlphaPlates (PerkinElmer) in a final volume of 25 µL, using an assay buffer composed of 25 mM HEPES (pH 7.4), 100 mM NaCl, and 0.005% Kathon. The DMSO concentration was kept constant at 5% (v/v) in all wells.

His-tagged LIFR (final concentration: 4.5 nM) was pre-incubated for 45 min under gentle agitation with serial dilutions of LRI-310 (10 concentrations ranging from 4.12 nM to 200 µM) or vehicle control. Subsequently, biotinylated LIF was added to each well (final concentration: 20 nM) and samples were incubated for an additional 15 min. His-tag acceptor beads (final concentration: 20 ng/µL) were then dispensed and incubated for 30 min, followed by the addition of streptavidin donor beads (20 ng/µL). Plates were protected from light and incubated for 3 h before signal acquisition on an EnSpire Alpha multimode plate reader (PerkinElmer).

2.5. Protein and ligand preparation

The X-Ray structure of human *h*LIFr (PDB code: 3E0G) was sourced from the RCSB PDB database and prepared using Protein Preparation Wizard [16] implemented in Maestro Suite ver. 2025–1, in order to automatically add hydrogen atoms, generate the appropriate protonation states at pH 7.4, assign bond orders and correcting residues with missing atoms. Finally, non-structural water molecules were removed and restrained minimization was applied to the heavy atoms to relieve steric clashes. The three-dimensional structure of compound LRI310 was generated using the graphical user interface (GUI) of Maestro ver. 2025-1 and its protonation state at pH 7.4 in water was calculated using the Epik module [17] Finally, the ligand was subjected to a minimization step using the OPLS2005 force field [18] through 2500 iteration steps of the Polak-Ribiere Conjugate Gradient (PRCG) algorithm [19].

2.6. Ligand docking procedure

The obtained structure of both *h*LIFR and LRI310 were then used for a two-step docking procedure successfully adopted in our previous work [15,20,21] characterized by hybrid QM/MM-based Quantum Polarized Ligand Docking (QPLD) method [22] as first step and a second step of

Induced-Fit Docking (IFD) [23]. The first approach was adopted to obtain the QM-derived ligand atomic charges at the B3LYP/6-31G* level in the protein environment that instead is described using the OPLS2005 force field. In this step, a first standard precision (SP) Glide docking was carried out, generating ten poses, and submitting the ligand to QM-ESP charge calculation. The resulting poses were then re-docked into the binding site using the Glide extra precision (XP) algorithm, employing the updated (QM-derived) partial charges to obtain more accurate docked poses ranked by GlideScore value. The centre of the grid box of size 10 × 10 × 10 Å was positioned on the centroid of the L2-L3 residues, to define the position and shape of all the L2-L3 residues, which were already characterized as putative binding site of EC359[24] to define the position and shape of all the L2-L3 binding pocket of *h*LIFR.

The most energetically favourable pose of LRI310 was submitted to the second IFD step, that was undertaken to consider the structural adaptation/flexibility of both ligand and L2-L3 loops of the protein. In this step, the extended sampling protocol was applied, generating up to 80 poses within an energy window of 2.5 kcal/mol for the ligand conformational sampling.

2.7. MTS cell proliferation assay

Cell viability was quantified using the CellTiter 96® Aqueous One Solution Cell Proliferation Assay (Promega, G5421). MIAPaCa-2 cells were seeded at 1 × 10^4 cells/well in 96-well plates. After 24 h of serum starvation (Day 1–2), cells were treated with LIF (10 ng/mL) either alone or together with LRI-310 (0.1–1–5-10–20-25 μM). On Day 3, MTS reagent was added according to the manufacturer's instructions, and absorbance at 490 nm was measured using a microplate reader.

2.8. Reverse and real time qPCR

After removing genomic DNA with DNase I (Thermo Fisher Scientific, Waltham, MA), 1–2 μg of total RNA from each sample was converted into cDNA using the FastGene Scriptase Basic Kit (Nippon Genetics, Mariaweilerstraße, Düren, Germany) in a final reaction volume of 20 μL. For quantitative PCR, 50 ng of the generated cDNA was amplified in a 20 μL reaction mixture containing 200 nM of each primer and 10 μL PowerUp™ SYBR™ Green Master Mix (Thermo Fisher Scientific, Waltham, MA). All reactions were performed in triplicate using a QuantStudio 3 system (Applied Biosystems, Foster City, CA) using the following thermal protocol: 95°C for 2 min, followed by 40 cycles at 95°C for 3 s and 60°C for 30 s. Relative gene expression was assessed using the ΔCt method. Primer sets were generated with the PRIMER3 software (http://frodo.wi.mit.edu/primer3/) using reference sequences obtained from the NCBI database. The forward and reverse primer sequences for the human genes were listed as follows:

ID Gene	Species	Sequence forward	Sequence reverse
GAPDH	*Homo sapiens*	*CAGCCTCAAGATCATCAGCA*	*GGTCATGAGTCCTTCCACGA*
Ki67	*Homo sapiens*	TGCTCTGGGTTACCTGGTCT	CAAAGGACACACGCCTTCTT
cMYC	*Homo sapiens*	TTTCGGGTAGTGGAAAACCA	CACCGAGTCGTAGTCGAGGT
VIM	*Homo sapiens*	TCAGAGAGAGGAAGCCGAAA	ATTCCACTTTGCGTTCAAGG
SNAIL	*Homo sapiens*	ACCCACACTGGCGAGAAG	TGACATCTGAGTGGGTCTGG
CEBPD	*Homo sapiens*	ATCGACTTCAGCGCCTACAT	GCCTTGTGATTGCTGTTGAA
IFI16	*Homo sapiens*	TCCAACTTTTCTGCTTTCGAC	TCATTGTTTCTCGGGTTTGTT
IFI30	*Homo sapiens*	TGGGCCACCAGTTAACTACA	CACCGCACAGTGCTTCATAG
BCL6	*Homo sapiens*	CTGCAGATGGAGCATGTTGT	TCTTCACGAGGAGGCTTGAT
SFN	*Homo sapiens*	AGAGCGAAACCTGCTCTCAG	CTCCTCGTTGCTTTTCTGCT
CSRP2	*Homo sapiens*	CACCTTGGAGACCGGATGT	GGATTTGTTGTAGGCCTGTGA
SNORA47	*Homo sapiens*	CACCGGTTAAGACCTCCAAA	AAATGTCGGCCAGCACAG
CLDN3	*Homo sapiens*	TTATCCGGGACTTCTACAACC	GACACGAGCAGCAGAGCA
SEMA3b	*Homo sapiens*	GGTCCCCAAGGGCAGTAG	CCGCGAGGCTACGTACAG
COL1a1	*Homo sapiens*	CCCAAGGCTTCCAAGGTC	GACCAGGTTTTCCAGCTTCC
ASMA	*Homo sapiens*	GTGTTCCCGTCCATCGTG	CTCTTGCTCTGAGCCTCGTC
TGFb	*Homo sapiens*	GGGATGGACAGATGGACAAC	GGGATGGACAGATGGACAAC
TIMP1	*Homo sapiens*	AGACGGCCTTCTGCAATTC	TCATAACGCTGGTATAAGGTGGT

2.9. LIFR transactivation assay

To evaluate LIFR-dependent STAT3 activation, HEPG2 cells were seeded into 24-well plates at 7.5 × 10^4 cells/well and incubated for 24 h. Cells were then co-transfected with plasmids encoding human LIFR (100 ng; OriGene RC226327), IL6ST/CD130 (100 ng; OriGene RC215123), the STAT3-responsive reporter plasmid pGL4.47[luc2P/SIE/Hygro] (200 ng; Promega E4041), and the Renilla control vector pGL4.70 (100 ng). After overnight recovery, cells were stimulated with LIF (10 ng/mL) alone or with increasing concentrations of LRI-310 (0.1–50 μM). Following 24 h of treatment, cells were lysed, and firefly and Renilla luciferase activities were measured using the Dual-Luciferase® Reporter Assay System (Promega). Firefly RLU values were normalized to Renilla RRU.

2.10. Western blot analysis

MIAPaCa-2 cells were plated in 6-well plates at a density of 1.5 × 10^6 cells per well and maintained in DMEM supplemented with 10% FBS, 1% L-glutamine, and 1% penicillin–streptomycin at 37 °C in a 5% CO_2 atmosphere. After 24 h of serum deprivation, cells were stimulated with LIF (10 ng/mL) either alone or in combination with LRI-310 (5 or 10 μM) for 10 min.

Cells were lysed in ice-cold RIPA buffer supplemented with protease and phosphatase inhibitors. Equal amounts of protein were resolved on 12% Tris-Glycine polyacrylamide gels (Invitrogen) and transferred onto nitrocellulose membranes. Membranes were incubated overnight at 4 °C with primary antibodies against STAT3 (1:500, Santa Cruz Biotechnology, sc-8019), phospho-STAT3 (1:1000, GeneTex, GTX118000), and Laminin (housekeeping control; appropriate dilution as per manufacturer's recommendation).

After incubation with HRP-conjugated secondary antibodies, signals were developed using Immobilon Western Chemiluminescent Substrate (MilliporeSigma) and imaged with the iBright Imaging System (Invitrogen). Densitometric analysis was performed using ImageJ, and STAT3 activation was expressed as the phospho-STAT3/total STAT3 ratio, normalized to Laminin levels.

2.11. Flow cytometry and IC-FACS analysis

MIAPaCa-2 cells were plated in 6-well plates at a density of 7×10^5 cells per well and cultured in DMEM supplemented with 10% FBS, 1% L-glutamine, and 1% penicillin–streptomycin at 37 °C in a 5% CO_2 atmosphere. After a 24-h serum-starvation period, cells were exposed to LIF (10 ng/mL) either alone or in combination with the LIFR antagonist LRI310 (10 μM) for 24 h.

For intracellular Ki-67 detection and cell-cycle analysis, cells were fixed for 30 min in the dark using IC Fixation Buffer (eBioscience™) and permeabilized with Permeabilization Buffer (10×, eBioscience™). Staining was then performed using the Ki-67 monoclonal antibody (clone SolA15) conjugated to Alexa Fluor™ 488 (eBioscience™). DNA content was simultaneously evaluated with 7-AAD to distinguish G0/G1, S, and G2/M cell-cycle phases.

Apoptosis was assessed by quantifying the sub-G0/G1 population and confirmed by 7-AAD-based discrimination of membrane-compromised cells.

Data acquisition was performed on an Attune NxT flow cytometer (Thermo Fisher Scientific) equipped with a standard 3-laser configuration. Analyses were conducted using FlowJo software (Tree Star), applying fluorescence-minus-one (FMO) controls to define gating boundaries. For each marker, the corresponding FMO sample contained all fluorochromes included in the test condition except the antibody of interest, allowing precise threshold determination.

2.12. Wound healing assay

MIAPaCa-2 cells were seeded in 24-well plates at 8×10^5 cells per well in complete DMEM and grown until reaching approximately 70–80% confluence. On the following day, a linear wound was generated by gently dragging a sterile 200-μL pipette tip across the centre of the monolayer. To avoid mechanical stress-induced detachment, scratches were performed without removing the culture medium. Wells were then rinsed twice with PBS to eliminate floating cells and debris, and fresh medium containing LIF (10 ng/mL) alone or in combination with LRI310 (10 μM) was added.

Immediately after scratch creation, wells were imaged under a phase-contrast microscope (T = 0 h). Cultures were then incubated for 24 h, after which a second set of images was acquired under the same conditions. Wound closure was quantified by measuring the area between the two edges of the scratch using image analysis software. All experiments were carried out in triplicate.

2.13. MIAPaCa-2/HPanSteC co-culture system

At Day 0, 6×10^4 of MIAPACA2 cells were plated in the insert of 12-well plate (Thermo Scientific, Cc Insert Md12 04My Dim 12/18 mm Pc Si 140652) with 500 μL DMEM. At Day 1, MIAPACA2 cells were starved for 24 h and in a new 12-well plate 1×10^5 HPanSteC cells were seeded in 700 μL of SteCM Medium. On Day 2, HPanSteC were subjected to a one-hour starvation period. Next, the inserts containing MIAPACA2 cells were combined with the wells, using an equal mix of medium from both cell lines, and subjected to the designed treatment: medium only, exposure to LIF 1o ng/mL, and LIF in combination with LRI 310 10 μM. On Day 3, RNA from both cell lines was isolated separately.

2.14. Statistical analysis

The distribution of each dataset was evaluated using both the Shapiro-Wilk test and the D'Agostino-Pearson omnibus test to assess normality. When comparing two independent groups, normally distributed variables were analysed using unpaired t-tests with Welch's correction, whereas non-normally distributed variables were evaluated using the Mann-Whitney *U* test. For experiments involving more than two conditions, parametric data were analysed by one-way ANOVA with Brown-Forsythe and Welch adjustments, while the Kruskal-Wallis test followed by Dunn's multiple-comparison procedure was applied to non-parametric datasets. Where appropriate, linear regression analyses were performed to examine the relationship between variables and trends across groups. All statistical analyses were conducted with GraphPad Prism version 10.6, and a p-value <0.05 was considered statistically significant.

3. Results

3.1. LIF reshapes the transcriptional landscape of MIAPaCa-2 cells toward pro-CAF signaling

To explore the transcriptional consequences of LIF stimulation in pancreatic cancer cells, we first confirmed basal LIFR and LIF expression in untreated MIAPaCa-2 cells by immunofluorescence (Fig. 1A). The Exposure to LIF (10 ng/mL, 24 h) markedly altered the global transcriptomic profile, as shown by the clear separation between untreated and LIF-treated cell in the Principal Component Analysis (PCA) plot (Fig. 1B). Transcriptome analysis identified 783 differentially expressed genes, of which 525 were downregulated and 258 upregulated (Fig. 1C). Pathway enrichment analysis revealed that LIF induced a transcriptional program consistent with stromal activation, with significant modulation of Interleukin (IL)-6 family Oncostatin M (OSM) and IL-11 signalling, interferon-gamma (IFNγ) related pathways, prostaglandin metabolism, endothelin signaling, Hippo-YAP activity and ECM-remodeling modules (Fig. 1D). Notably, OSMR and SOCS family members, which participate in multiple stromal-related circuits, were consistently upregulated.

A targeted gene-level analysis was conducted analysis was performed on the 30 most upregulated and 30 most downregulated transcripts identified by RNA-seq Fgure_1E), annotating each gene through a structured literature search focused on fibroblast biology, extracellular matrix remodeling and CAF activation. This curation revealed that many LIF-responsive genes clustered within stromal programs. Based on this curation, genes were grouped into the functional categories shown in Fig. 1F: iCAF-associated inflammatory signaling (light blue), CAF-activating paracrine cues (orange), ECM/adhesion–mechano-transduction (myCAF-biased) (green), Ribosome/RNA-processing shift (pink/black), Stromal-inhibitory cues (violet). The exposure to LIF resulted in a marked enrichment of iCAF-associated inflammatory mediators, including *CCAAT/enhancer-binding protein delta* (CEBPD), an IL-1/IL-6–inducible transcription factor that amplifies inflammatory cytokines [25]; Alpha protein kinase 1 (ALPK1), a kinase operating upstream of NF-κB through the ALPK1–TIFA axis [26]; and the interferon-regulated genes Interferon gamma-inducible protein (IFI)-16, IFI30 and *Guanylate-binding protein 3* (GBP3), all linked to IFN-driven inflammatory states and inflammasome activation [27,28]. Alongside these inflammatory cues, LIF upregulated several CAF-activating paracrine mediators, *including C-C motif chemokine ligand 5* (CCL5), a potent chemoattractant that promotes fibroblast recruitment and activation via CCR5 [29]; *Carboxypeptidase X member 1* (CPXM1), implicated in ECM remodeling and stromal activation [30]; and *C1q and TNF related protein 3* (C1QTNF3) (CTRP3), an adipokine capable of modulating fibroblast proliferation and matrix deposition in TGF-β–responsive contexts [31]. LIF also induced transcripts involved in ECM organization, adhesion and mechano-transduction, features associated with myCAF-biased phenotypes. These included SFN (14–3-3σ), which interfaces with TGF-β/Smad and cytoskeletal pathways to sustain fibrotic programs [32]; *Cysteine- and glycine-rich protein 2 (*CSRP2), an actin-binding protein that stabilizes stress fibres and focal adhesions [33]; and *Claudin-3 (*CLDN3), a tight-junction component linked to EMT and Wnt/β-catenin signaling with relevance to epithelial–stromal crosstalk [34]. *Protease-activated receptor 1* (PAR1/F2R), also upregulated, contributes to this module through thrombin-dependent induction of myofibroblastic differentiation and ECM contraction [35].

In addition to genes promoting stromal activation, LIF suppressed

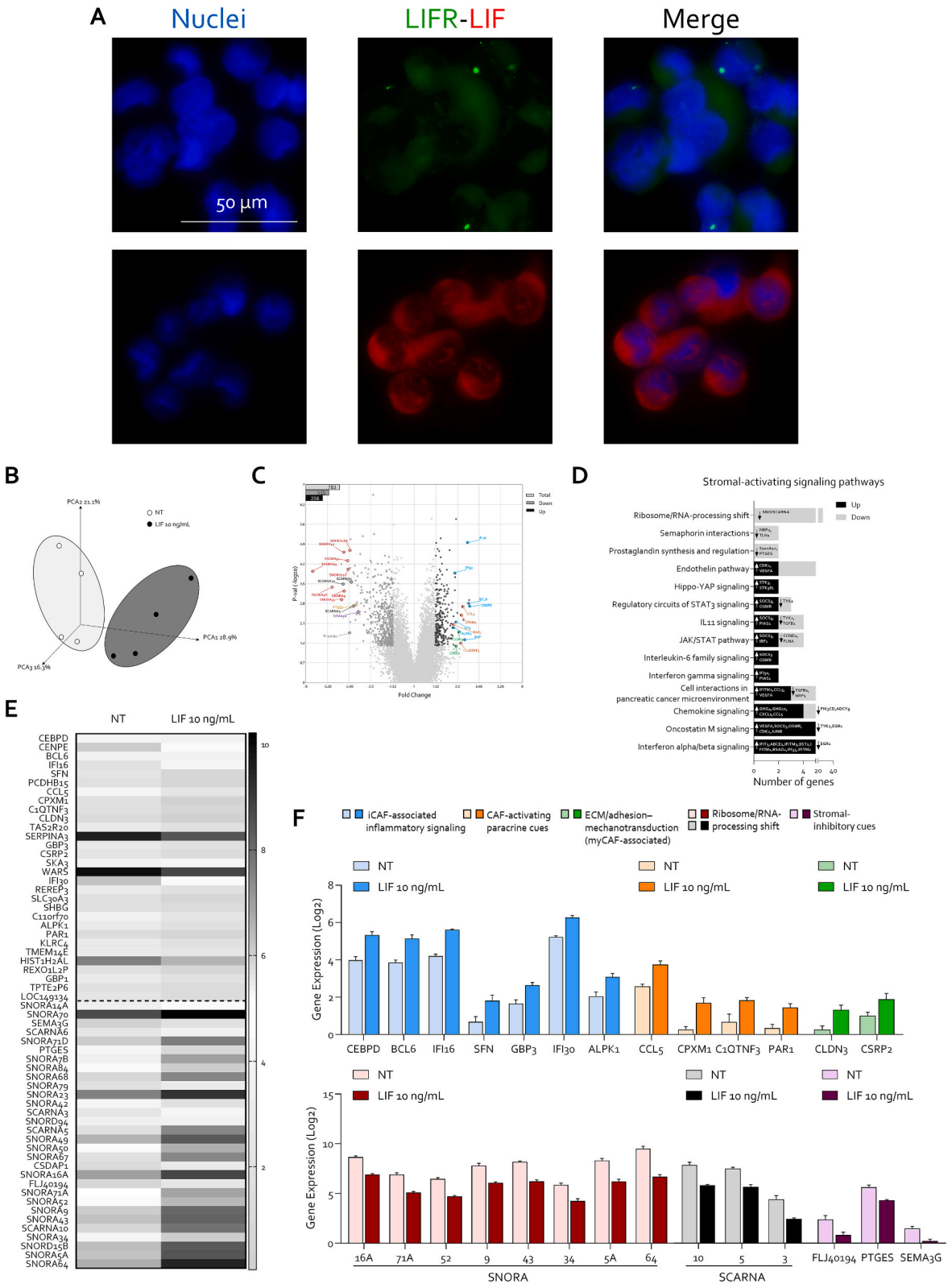

Fig. 1. LIF treatment reshapes the transcriptomic profile of MIAPaCa-2 cells toward a stromal-activating program. (A) Representative immunofluorescence images of untreated MIAPaCa-2 cells showing basal expression of LIFR (green) and LIF (red); nuclei were counterstained with DAPI (blue). MIA-PaCa-2 cells were exposed to 10 ng/mL of LIF for 24 h. then RNA was extracted and Transcriptome analysis was performed. (B) Principal Component Analysis (PCA) plot (C) Volcano plot of differentially expressed genes (DEGs) (D) *Per pathway* analysis. (E) Heatmap showing the expression profile of the 30 most upregulated and the 30 most down-regulated transcripts identified by RNA-seq in MIAPaCa-2 cells cultured under basal conditions (NT) or after 24 h of stimulation with LIF (10 ng/mL). Each row represents a single gene ranked by fold change, with darker shades indicating higher expression levels. (F) Selected up- and downregulated genes among the top 30 DEGs, grouped into functional categories related to CAF activation: CAF-activating paracrine cues, iCAF-associated inflammatory signaling, ECM/adhesion–mechanotransduction (myCAF-biased), loss of stromal-inhibitory cues, and ribosome/RNA-processing shift. Each value was the mean ± SEM of 4 samples per group. Fold change > 2, $p < 0.05$.

transcripts whose functions are typically stromal-inhibitory, including *Semaphorin 3G* (SEMA3G), an anti-angiogenic semaphorin that limits cell migration and vascular/ECM remodeling [36], and *Prostaglandin E synthase (*PTGES), which encodes prostaglandin E synthase; its product PGE_2 is known to restrain fibroblast-to-myofibroblast transition via EP2/cAMP signaling, its downregulation therefore suggests removal of a brake on myCAF differentiation [37]. LIF further reduced a broad cluster of *Small nucleolar RNA* (snoRNA) and *Small Cajal body-specific RNA* (scaRNA) species (SNORA, SNORD, SCARNA), reflecting a broader ribosome/RNA-processing shift associated with secretory and highly interactive cellular states.

Altogether, this curated gene-level analysis indicates that LIF elicits a coordinated transcriptional response in MIAPaCa-2 cells, integrating inflammatory, paracrine and mechano-transductive pathways with suppression of stromal-restraining cues, collectively recapitulating canonical features of CAF-activating programs.

3.2. Increased LIF expression associates with stromal activation and pro-CAF gene signatures in human PDAC

To determine whether LIF or its receptor are expressed within the stromal compartment of human pancreatic tumors, immunofluorescence staining for α-SMA, LIF and LIFR was performed on PDAC samples from our internal cohort (Fig. 2). In all cases, α-SMA highlighted the presence of a dense population of activated fibroblasts surrounding neoplastic structures.

Dual staining for α-SMA and LIF showed minimal spatial overlap, indicating that LIF protein is not predominantly localized within α-SMA^+ stromal cells. In contrast, the combination of α-SMA and LIFR revealed a clear and consistent colocalization pattern, with LIFR signal enriched in α-SMA^+p fibroblasts across multiple regions of the tumor microenvironment.

This differential distribution suggests that, within human PDAC, LIFR is expressed on activated stromal fibroblasts, whereas LIF appears to derive primarily from non-α-SMA^+ compartments. These observations support the hypothesis that fibroblasts in the PDAC microenvironment may respond to exogenous or tumor-derived LIF through stromal LIFR engagement.

To evaluate whether the stromal-activating transcriptional program observed in MIAPaCa-2 cells is also detectable in human pancreatic cancer, the GSE196009 dataset was analysed (Fig. 3).

LIF expression was significantly increased in PDAC samples compared with non-neoplastic tissue, whereas LIFR expression was markedly reduced, indicating an opposite regulation of ligand and receptor within the tumour microenvironment (Fig. 3A).

A manual deconvolution strategy was then applied to infer the relative abundance of epithelial cells, CAFs, myCAFs and iCAFs based on curated marker sets. For each sample, the expression of epithelial cells, CAFs, myCAFs and iCAFs was inferred by calculating the average expression of established marker genes for each cell type. Epithelial features were assessed by integrating EPCAM, KRT19, MUC1, KRT14 and KRT17. CAF enrichment was estimated using PDGFRB together with COL1A1, COL1A2 and COL3A1. myCAF-associated transcripts were derived from ACTA2, TAGLN, MYL9, TPM1 and ITGA11, whereas the iCAF signature was constructed from CXCL1, CXCL2, CXCL5, CCL2, PTGS2, IL1R1 and OSMR. This approach allowed us to reconstruct the major stromal components from bulk-gene expression data. The analysis showed a reduction in epithelial markers and a clear enrichment of CAF-, myCAF- and iCAF-associated transcripts in PDAC tissue compared with non-neoplastic samples (Fig. 3B).

Key stromal-activating genes, including ACTA2, TGFB1, COL1A1, COL1A2, COL3A1, and OSMR, were significantly increased in PDAC (Fig. 3C), consistent with enhanced fibroblast activation and extracellular matrix remodeling. A PCA constructed from these stromal signatures showed a clear separation between neoplastic and non-neoplastic tissues (Fig. 3E), confirming the overall divergence in microenvironmental transcriptional states.

We next examined the expression of stromal-modulating genes previously identified in the MIAPaCa-2 RNA-seq dataset (Fig. 1). Several of the upregulated candidates such as IFI16, SFN, IFI30, CPXM1, C1QTNF3 and CLDN3, were similarly increased in PDAC compared to non-neoplastic samples (Fig. 3F), supporting their relevance in human tumors. Among the downregulated transcripts, SNORA47, SEMA6A and SEMA6D showed reduced expression in PDAC, whereas other snoRNA and scaRNA species exhibited minimal variation (Fig. 3D).

Correlation analyses between LIF/LIFR and the deconvoluted cell-type signatures demonstrated a direct association between LIF and CAF, myCAF and iCAF scores in PDAC, whereas this relationship was not evident in non-neoplastic tissues, where LIFR correlated more strongly with stromal signatures (Fig. 3E–G). At the gene level, LIF expression correlated with several stromal-activating transcripts including BCL6, IFI16, IFI30, CPXM1, C1QTNF3 and CSRP2, while the downregulated genes SNORA47, SEMA6A and SEMA6D showed a direct correlation with LIFR but not with LIF.

Together, these findings indicate that the LIF-associated stromal program characterized in vitro is reflected in human PDAC, where LIF and LIFR show distinct associations with fibroblast subsets and stromal-remodeling genes.

3.3. Pharmacological targeting of LIFR reveals LRI310 as a direct inhibitor of LIF–LIFR binding

The evidence that LIF promotes a stromal-activating transcriptional program in MIAPaCa-2 cells and correlates with CAF, myCAF and iCAF signatures in human PDAC prompted us to investigate whether pharmacological targeting of the LIF–LIFR axis could interfere with this pathway. Previous similarity-based screening of FDA-approved molecules, performed using the structure of the reference LIFR antagonist EC359, identified mifepristone as the closest pharmacophore [38], supporting the feasibility of steroid-derived scaffolds for LIFR inhibition. Building on these pharmacological and structural insights, we synthesized the LRI series [15] of LIFR-targeting molecules and selected LRI310 for biochemical and computational characterization (Fig. 4A).

To determine whether LRI310 directly interferes with ligand–receptor engagement, we performed an AlphaScreen® proximity assay using recombinant human LIF and the extracellular domain of LIFR. LRI310 produced a concentration-dependent reduction in LIF/LIFR complex formation, with an IC_{50} of approximately 0.4 μM (Fig. 4B). These data indicate that LRI310 acts as a direct antagonist of LIFR by impairing the physical interaction between LIF and its receptor.

Subsequently, the best ranked QPLD pose of compound LRI310 in complex with *h*LIFR (PDB ID: 3E0G) was explored by applying the same computational strategy previously reported in earlier studies [15,20,21]. The LIF binding site is positioned across the extracellular D1–D5 domains, more specifically in an area delimited by three highly flexible loops: L1, located in the Ig-like D3 domain, and L2 and L3, embedded in the cytokine-binding D4 domain (Fig. 4A) [39]. To take into account the marked flexibility of the orthosteric binding cavity in the definition of LRI310 binding mode, we implemented a two-step docking protocol. Initially, a rigid docking was carried out through the QPLD module of Maestro (Schrödinger Inc.), setting the docking grid between domains D3 and D4, encompassing loops L1-L3. The QPLD stage positioned LRI310 within a narrow pocket framed by loops L2 and L3, consistent with binding modes described for other LIFR antagonists, including EC359, mifepristone and bile acids derivativities[20,38]. Next, the top-ranked QPLD pose was refined using an Induced Fit Docking (IFD) procedure (Schrödinger Inc.). As in our previous studies on LRI family of compounds [15,20], two leading conformations, pose A and pose B, were observed from the IFD (Fig. 4D–E). The two IFD poses mainly differed in the orientation of the steroidal scaffold within the pocket, influenced by alternative spatial arrangements of loops L2 and L3. In case of LRI310, pose A (Fig. 4D) emerged as the most energetically

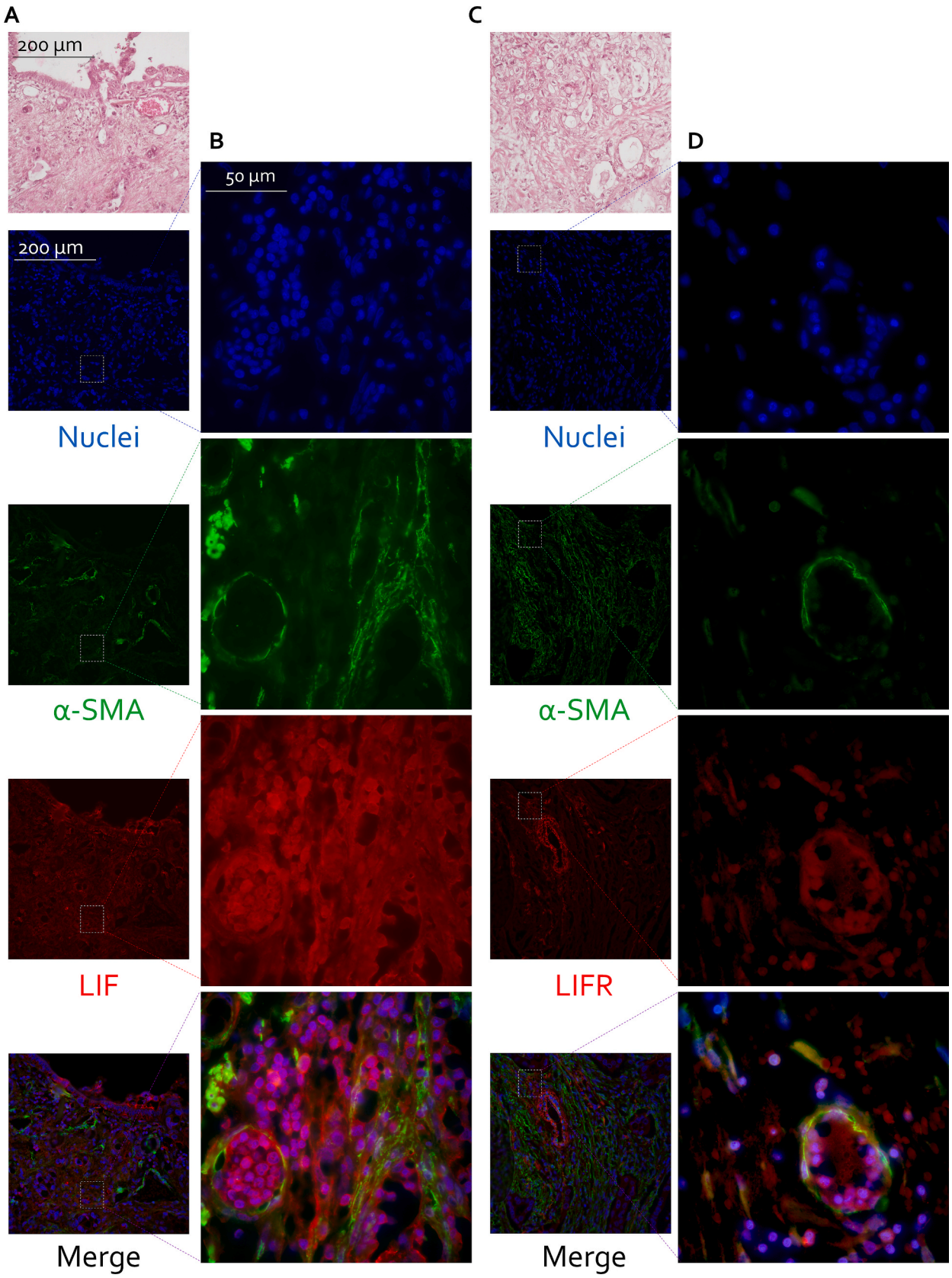

Fig. 2. LIFR identifies α-SMA^{+} stromal fibroblasts in human PDAC. Representative histological and immunofluorescence images from our internal PDAC patient cohort. (A) H&E staining and (B) α-SMA (green) and LIF (red); (C) H&E staining and D) α-SMA (green) and LIFR (red) Nuclei were counterstained with DAPI (blue). Scale bars indicated in panels.

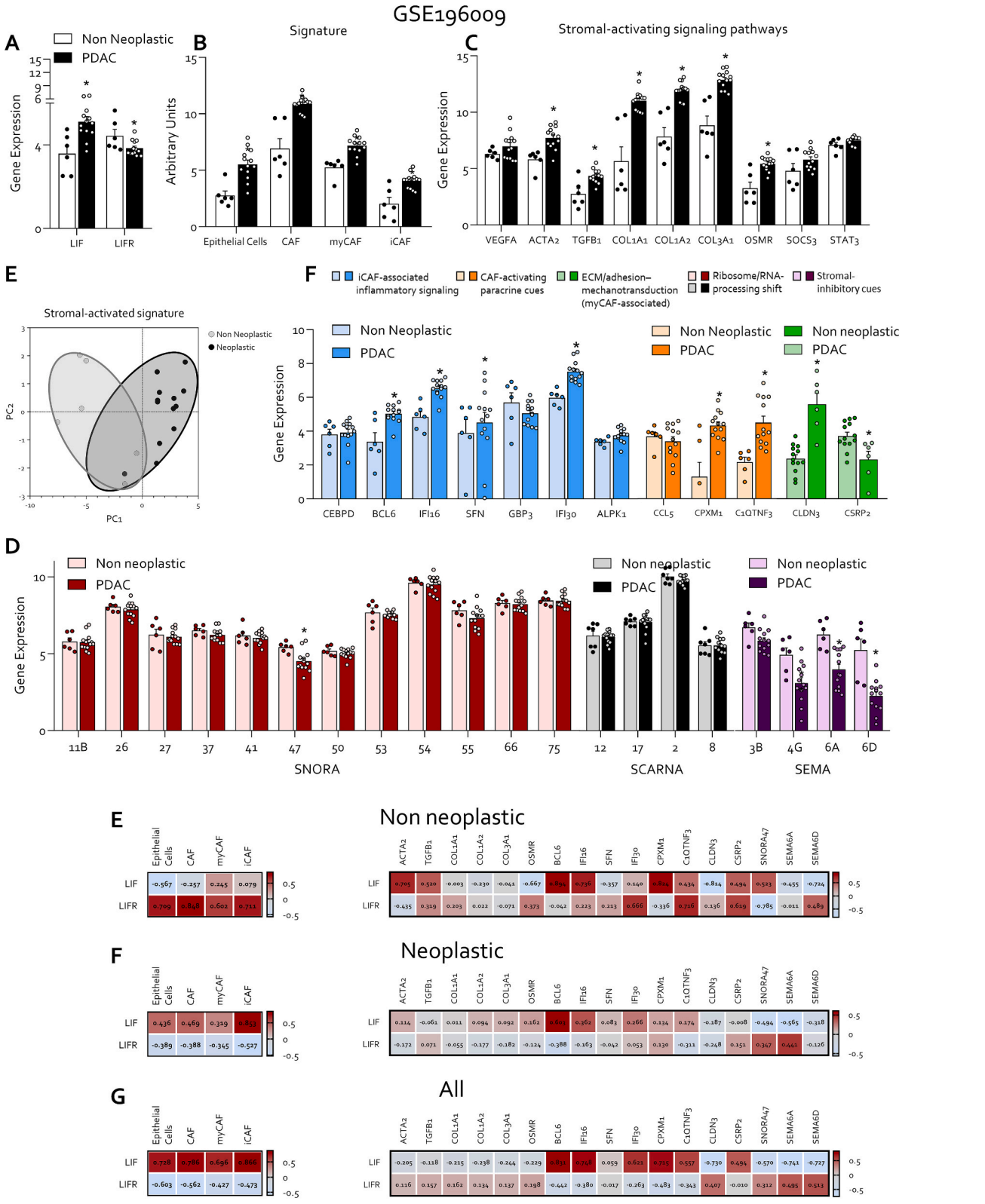

Fig. 3. Analysis of the GSE196009 dataset reveals stromal and fibroblast-associated signatures enriched in PDAC. (A) LIF and LIFR expression in non-neoplastic and pancreatic ductal adenocarcinoma (PDAC) samples. (B) Manual gene-set deconvolution of epithelial cells, CAFs, myCAFs and iCAFs. (C) Expression of stromal-activating signaling pathway genes. (E) PCA based on stromal-activation genes. (F–D) Expression of selected stromal-modulating genes identified in the MIAPaCa-2 RNA-seq dataset categorized into iCAF-associated inflammatory signaling(light blue), CAF-activating paracrine cues (orgnge), ECM/adhesion–mechanotransduction (green), ribosome/RNA-processing shift (pink/black) and stromal-inhibitory cues (violet). (E–G) Correlation heatmaps showing associations between LIF/LIFR and epithelial, CAF, myCAF and iCAF signatures, as well as with individual stromal-modulated genes. *p < 0.05.

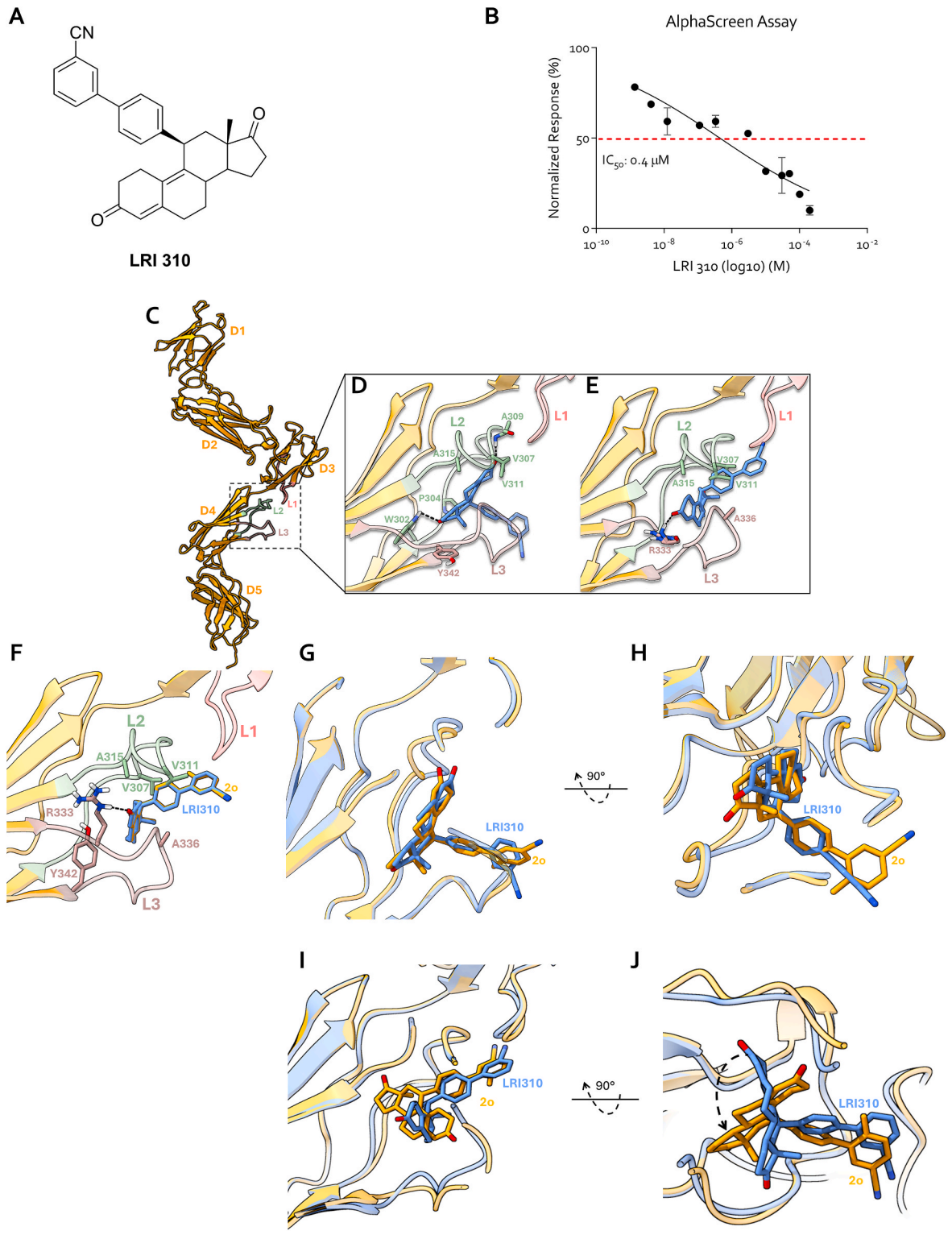

Fig. 4. LRI310 inhibits LIF–LIFR binding and adopts two alternative binding modes within the LIFR cytokine-binding pocket. (A) Chemical structure of LRI310. (B) AlphaScreen® assay showing the inhibitory activity of LRI310 on LIF–LIFR binding and corresponding IC_{50}. (C) Extracellular segment of hLIFR D1–D5 domains (PDB ID: 3E0G) used for docking calculations, with a focus on the ligand binding site defined by loop L1 (pink cartoon) of the Ig-like domain D3, and loops L2 (green cartoon), and L3 (brown cartoon) of the D4 domain; (D) Best ranked IFD pose (pose A) of LRI310 (cyan stick) within the L2-L3 loops engaging one hydrogen bond with W302. (E) Second best ranked IFD pose (pose B) of LRI310 (cyan stick) with the biphenyl moiety pointing towards the L1 loop and the steroidic scaffold engaging one hydrogen bond with R333. Hydrogen bond interactions are depicted as dashed black lines. (F) Superposition of the best GlideScore ranked QPLD pose of LRI310 (cyan stick) and compound 2o (orange stick). (G) Front view of the best ranked IFD pose (pose A) of LRI310 (cyan stick) superimposed to pose B of compound 2o (orange stick). (H) The rotated view of the two IFD poses highlights the very similar orientation of the steroidic scaffold and the different orientation of the biphenyl moiety. (I) Front view of the second best ranked IFD pose (pose B) of LRI310 (cyan stick) superimposed to pose A of compound 2o (orange stick). (J) The rotated view of the two IFD poses highlights the very similar orientation of the biphenyl moiety and the different orientation of the steroidal scaffold.

favoured. The binding mode was mainly stabilized by hydrophobic contacts with the two hydrogen bonds, involving both the oxygen atom of the carbonyl groups in rings A and D, respectively with the backbone of the A309, and the second involving W302. Key hydrophobic contacts included interactions between ring A and V307/V311, ring B and T316, ring D and L331/Y342, while the biphenyl moiety engages hydrophobic contact with P304 and the methylene groups of E340. Compared to the parent compound **2o** described in our previous work [15], the lack of the ortho methyl group on the distal phenyl ring of the biphenyl moiety influenced the overall conformation of the biphenyl ring favouring a different angle between the two aromatic rings (Fig. 4F–J). Although this conformational change did not significantly affect the global binding pose of LRI derivatives, it may have influenced apolar interactions mediated by the distal ring, partly due to changes in electron density resulting from the lack of the methyl substituent. Taken together, these structural differences may explain the reduced activity of LRI310 compared to compound **2o**.

3.4. LRI310 antagonizes LIF-driven proliferative, pro-survival and pro-migratory programs in PDAC cells

To investigate the functional consequences of LIFR blockade, MIAPaCa-2 cells were challenged with LIF and increasing concentrations of LRI310. In MTS assays, LIF markedly enhanced cell viability, whereas co-treatment with LRI310 produced a concentration-dependent suppression of this proliferative effect, yielding an IC_{50} of approximately 0.2 μM (Fig. 5A). Consistently, LRI310 blunted the transcriptional induction of key proliferation and EMT-associated genes such as KI67, cMYC, VIM and SNAI1, elicited by LIF (Fig. 5B). Immunofluorescence analysis confirmed a reduction in Ki-67–positive nuclei upon LRI310 exposure, fully reversing the increase observed under LIF stimulation (Fig. 5C). Because LIF signals through JAK/STAT pathways, we next assessed STAT3 activation. LIF robustly increased STAT3 phosphorylation, whereas LRI310 inhibited this response with a clear dose dependence and maximal suppression at 10 μM (Fig. 5D–E), indicating effective blockade of LIFR downstream signaling and comparable to the reported effects of the reference LIFR antagonist EC359 [24]. Cell-cycle analysis further demonstrated that LIF promotes progression into S-G_2-M and reduces the resting G_0–G_1 compartment. These effects were reverted by LRI310, which restored G_0-G_1 accumulation and significantly increased the proportion of apoptotic cells (Fig. 6A and B). In parallel, LRI310 mitigated LIF-induced cytoskeletal remodeling, reducing vimentin assembly and fluorescence intensity (Fig. 6C), consistent with a reversal of EMT-like features. Given that LIF favored acquisition of a migratory phenotype, we evaluated cell motility using wound healing assays. LIF stimulation enhanced migration and accelerated wound closure, whereas co-treatment with LRI310 significantly impaired this effect, reducing wound closure to near-basal levels (Fig. 6D).

Collectively, these findings demonstrate that LRI310 effectively counteracts LIF/LIFR signaling in pancreatic cancer cells, suppressing proliferative, survival, EMT and migratory pathways that contribute to PDAC aggressiveness.

3.5. LIF-dependent epithelial-stromal communication induces pro-CAF programs in co-culture and is reversed by LIFR blockade

Given the evidence that LIF reshapes the transcriptional landscape of MIAPaCa-2 cells toward a stromal-activating phenotype and that, in human PDAC, LIFR is predominantly expressed on α-SMA^+ fibroblasts, we investigated whether LIF-driven epithelial signals could directly modulate pancreatic stellate cell activation. Confocal imaging of HPanSteC confirmed this premise: stellate cells displayed robust α-SMA and LIFR expression, whereas LIF immunoreactivity was minimal under basal conditions (Fig. 7A), supporting the notion that LIF is principally of epithelial origin while its receptor resides on stromal cells.

To model this epithelial-stromal axis, MIAPaCa-2 and HPanSteC were placed in transwell co-culture and exposed to LIF with or without pharmacological blockade of LIFR (Fig. 7B). After 24 h, RNA was extracted separately from each compartment to dissect cell type-specific transcriptional responses.

In MIAPaCa-2 cells, LIF stimulation reproduced the transcriptional features identified in our RNA-seq dataset, with significant induction of *CEBPD, IFI16, IFI30* and *BCL6*, key components of the inflammatory and interferon-related circuitry associated with iCAF-like programs (Fig. 7C). Consistent with LIFR antagonism, this transcriptional activation was markedly blunted when the interaction between LIF and LIFR was inhibited, confirming that these epithelial outputs depend on intact LIF–LIFR signaling. Conversely, *SNORA47,* one of the small nucleolar RNAs downregulated by LIF in monoculture, was further restored upon LIFR inhibition, in line with the reversal of the ribosome/RNA-processing shift previously described.

Strikingly, the stromal compartment responded to epithelial LIF exposure with a clear activation profile. In HPanSteC, LIF significantly increased the expression of prototypical myofibroblast and matrix-remodeling markers including *COL1A1, ACTA2 (α-SMA), TGFB1* and *TIMP1*, consistent with high responsiveness of fibroblasts to epithelial-derived LIF (Fig. 7D). Blockade of LIFR suppressed this activation program, restoring gene expression levels toward those observed under basal co-culture conditions.

Together, these findings demonstrate that LIF orchestrates a bidirectional communication between pancreatic cancer cells and stromal fibroblasts, promoting inflammatory and matrix-remodeling programs in both compartments. Importantly, these effects are fully dependent on LIF-LIFR engagement, as pharmacological interruption of this axis reverses LIF-induced transcriptional activation in tumor cells and stellate cells alike. This co-culture system therefore recapitulates the epithelial-stromal circuit inferred from our transcriptomic and patient-derived data and provides functional evidence that LIFR antagonism can effectively disrupt pro-fibrotic and pro-tumorigenic signaling in the PDAC microenvironment.

4. Discussion

Leukaemia inhibitory factor (LIF) is increasingly recognised as a central node in the cytokine networks that sustain PDAC progression [12]. Beyond its classical roles in development and stem cell biology, LIF is aberrantly produced in several solid tumours, where it promotes proliferation, epithelial–mesenchymal transition (EMT), metastatic dissemination and chemoresistance through activation of the LIFR–gp130–JAK/STAT3 axis [9,13,40–44]. In PDAC, LIF expression is elevated in tumour tissue and in circulation, associates with poor prognosis and has been implicated in tumour–stroma crosstalk [45–47]. Building on this background and on our previous published studies [15,38,48] the present study delineates a previously unappreciated function of LIF as an epithelial driver of cancer-associated fibroblast (CAF) programming and identifies the small molecule LRI310 as a direct inhibitor of LIF:LIFR interaction capable of disrupting these pro-fibrotic circuits.

The unbiased transcriptomic analysis in MIAPaCa-2 cells shows that short-term LIF exposure is sufficient to rewire the epithelial transcriptome toward a stromal-activating configuration. In addition to broadly modulating IL-6 family, interferon-related, prostaglandin and Hippo–YAP pathways, LIF induced a compact set of genes with well-established roles in fibroblast activation, extracellular matrix remodelling and inflammatory signalling. The curated categorisation of the 30 most upregulated and 30 most downregulated genes reveals a coordinated enrichment in iCAF-associated inflammatory mediators (*CEBPD, ALPK1, IFI16, IFI30, GBP3*), CAF-activating paracrine cues (*CCL5, CPXM1, C1QTNF3*), and ECM/adhesion-mechanotransduction modules biased toward myCAF phenotypes (*SFN, CSRP2, CLDN3, PAR1/F2R*). In parallel, LIF repressed stromal-restraining components, including the

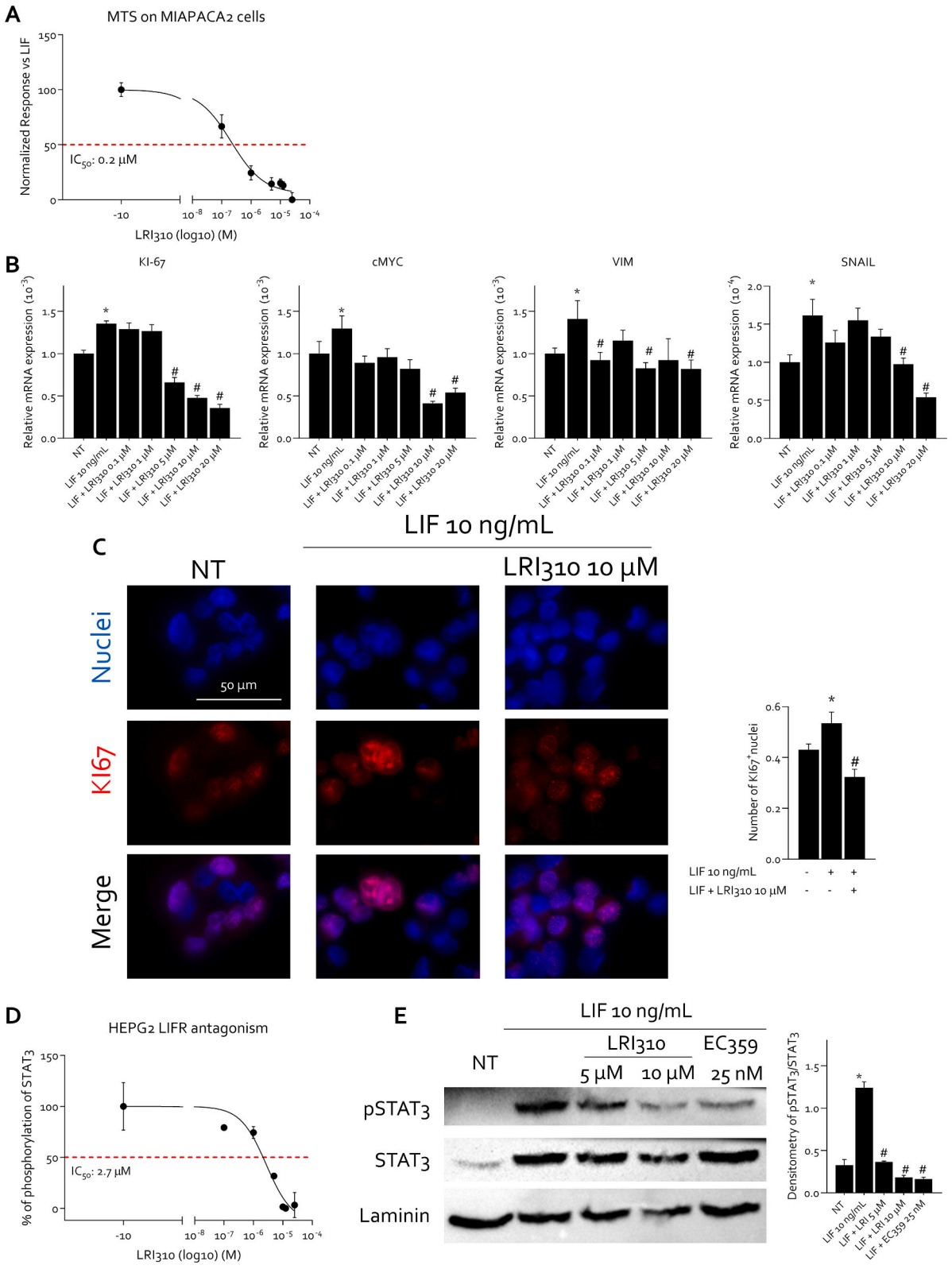

Fig. 5. LRI310 counteracts LIF-induced proliferation in a STAT3 depemdent manner on MIAPaCa-2 cells. MIAPACA2 was exposed to LIF (10 ng/ml), alone or with 0.1, 1, 5, 10 and 20 µM of LRI310, cells were compared with untreated controls (NT). (A) Concentration-response curve of LRI310 was determined using MTS assay on MIA PaCa-2 cells (n = 10). (B) Relative mRNA expression of *Ki-67, cMYC, VIM, SNAIL* in MIAPACA2 cells. Each value was normalized to GAPDH. (n = 5) (C) Immunofluorescence staining of Ki67 (red) in MIAPACA2 cells with quantification of number of Ki67^{+} nuclei. (D) STAT3 transactivation on HepG2 cells of LRI310. (E) In another experimental cells MIAPACA2 was exposed to LIF (10 ng/ml), alone or with 5, 10 and 20 µM of LRI310 and 25 nM of EC359 cells were compared with untreated controls (NT). Representative Western blot analysis of phospho (p)-STAT3 and STAT3, LAMININ proteins. Densitometric analysis demonstrating p-STAT3/STAT3.

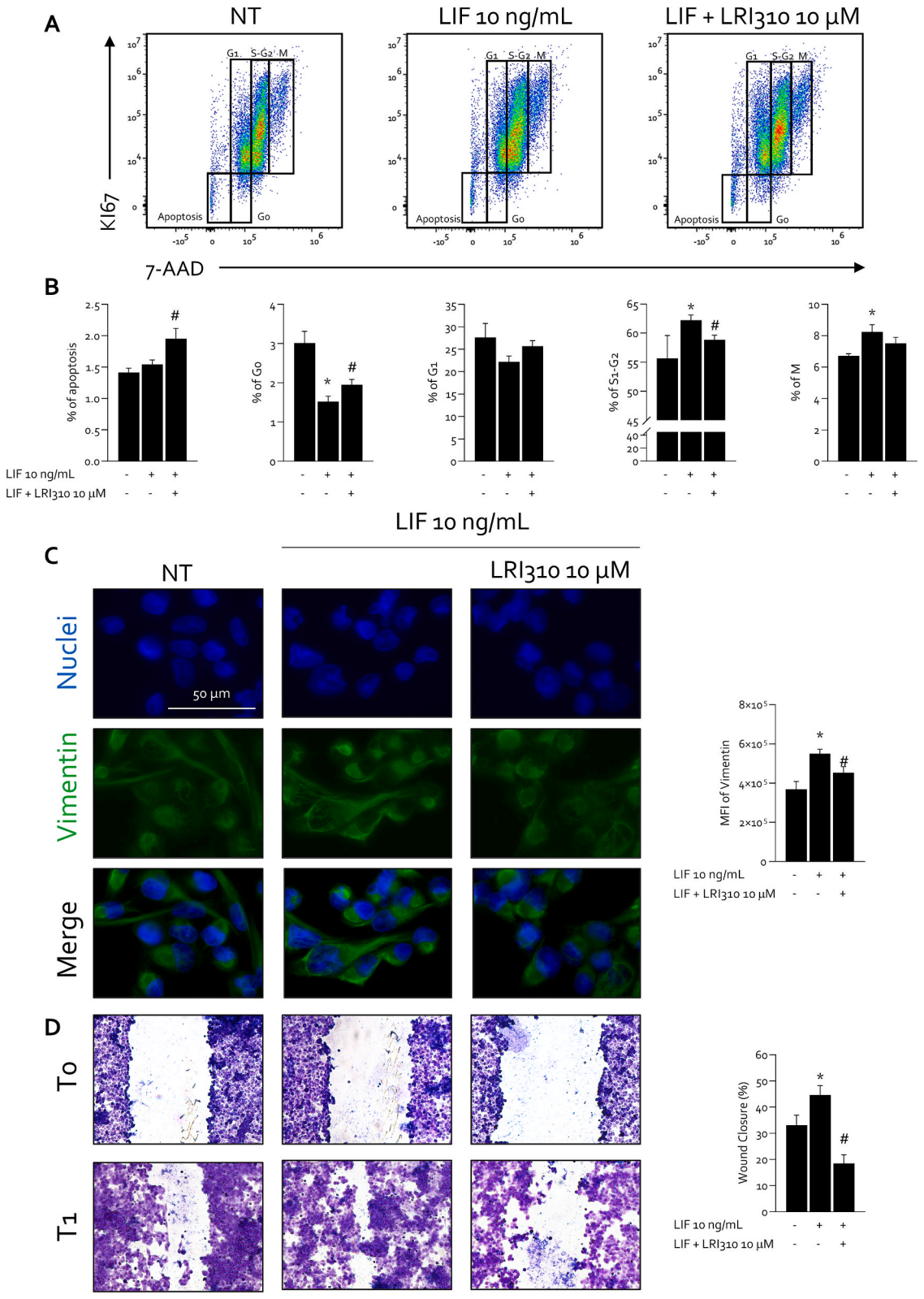

Fig. 6. LRI310 modulates cell cycle progression, apoptosis, EMT markers and migration in MIAPaCa-2 cells. (A) Cell cycle phase analysis was performed by Ki-67/7-AAD staining through IC-FCM. (B) Frequencies of Apoptotic cells, Resting cells (G0-G1 phase) and Proliferating cells (S-G2 phase) and Mitotic phase (M phase) in NT, LIF 10 ng/mL and LIF + LRI-310 10 µM experimental groups. (C) Immunofluorescence staining of Vimentin (green) in Mia Paca with quantification of Vimentin corrected total cell fluorescence (CTCF). (D) A scratch wound healing assay is shown. MIAPACA2 cell monolayers were scraped in a straight line using a p200 pipette tip, then they are left untreated or primed with LIF 10 ng/mL alone or in combination with LRI-310 10 µM. The wound generated was captured at 0 h and 24 h of incubation with the compounds above described. The images show cell migration at the two times points indicated and percentage of wound closure at 24 h. In each experimental set results are the mean ± SEM of 5 samples for groups. (E) Wound closure in percentual.

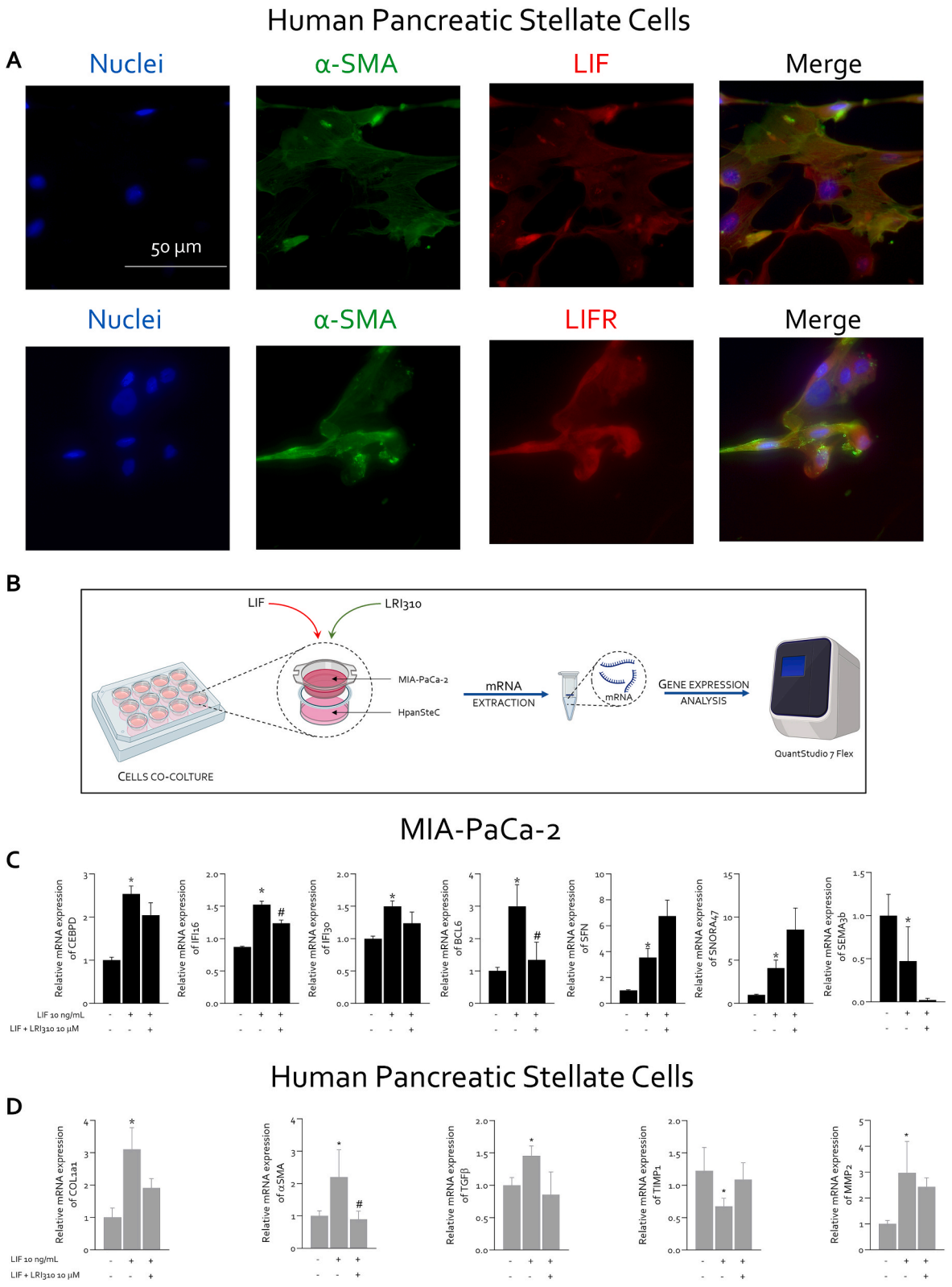

Fig. 7. LIF/LIFR-dependent crosstalk between pancreatic cancer cells and human pancreatic stellate cells is reversed by LIFR antagonism. (A) Representative confocal images of human pancreatic stellate cells (HPanSteC) showing nuclear staining, α-SMA, and either LIF or LIFR immunoreactivity under basal conditions. (B) Schematic representation of the transwell-based co-culture system used to interrogate epithelial–stromal communication between MIAPaCa-2 cells and HPanSteC. (C) Gene expression analysis of MIAPaCa-2 cells following 24 h co-culture under basal conditions, LIF stimulation (10 ng/mL), or LIF plus LIFR antagonist, LRI310 (10 µM). (D) Gene expression analysis of HPanSteC harvested from the corresponding co-cultures. In each experimental set results are the mean ± SEM of 5 samples for groups. Each value was normalized to GAPDH.

anti-angiogenic semaphorin *SEMA3G* and *PTGES*, whose product PGE_2 physiologically limits fibroblast-to-myofibroblast transition. together with a broad cluster of sno/scaRNAs consistent with a shift toward a highly secretory state. These findings extend previous RNA-seq studies, in which LIF/LIFR antagonism primarily emerged as a regulator of cell-cycle progression, DNA replication and apoptosis in PDAC cells [20]. Here we show that, even in the absence of stromal cells, LIF imprints an epithelial transcriptional program that is heavily "pre-wired" toward CAF activation.

The relevance of this pro-CAF signature was corroborated by analyses of human PDAC specimens. Immunofluorescence mapping in our internal cohort revealed that LIFR colocalises with α-SMA in stromal fibroblasts, whereas LIF protein is largely confined to non-α-SMA^+ compartments, supporting a model in which tumour or epithelial cells act as the primary source of LIF, while the receptor is enriched on activated stromal cells. This spatial segregation is mirrored at the transcriptomic level in the GSE196009 dataset, where *LIF* is upregulated whereas *LIFR* is downregulated in bulk PDAC compared with non-neoplastic tissue. Manual deconvolution of bulk gene expression, based on established epithelial, CAF, myCAF and iCAF markers, revealed a profound remodelling of tissue composition, with loss of epithelial signatures and expansion of all CAF subsets in tumour samples. Within this stromal-enriched context, key profibrotic mediators such as *ACTA2, TGFB1, COL1A1/2, COL3A1* and *OSMR* were significantly increased.

Importantly, several LIF-responsive genes identified in MIAPaCa-2 cells including *IFI16, SFN, IFI30, CPXM1, C1QTNF3 and CLDN3*, were likewise upregulated in PDAC tissue, while *SNORA47*, *SEMA6A* and *SEMA6D* were reduced, supporting the translational relevance of the epithelial LIF signature.

Correlation analyses further reinforced the notion of an active LIF–stroma axis: in PDAC, LIF expression correlated positively with CAF, myCAF and iCAF scores and with stromal-activating genes such as *BCL6, IFI16, IFI30, CPXM1, C1QTNF3* and *CSRP2,* whereas in non-neoplastic tissues these associations were diminished and LIFR, rather than LIF, showed stronger relationships with stromal features.

Together, these observations position LIF as a stromal-sensitising cue whose abundance tracks with the expansion and activation status of CAF populations in human PDAC.

Having established that LIF can shape epithelial and stromal transcriptional landscapes, we next sought to pharmacologically intercept this axis. Our previous work showed that the EC359 pharmacophore can be used to identify steroidal LIFR binders, including mifepristone and the dual FXR/GPBAR1 agonist BAR502, that behave as competitive antagonists of LIF-LIFR binding, attenuating STAT3 activation and reversing EMT, proliferative and migratory responses in PDAC models [38,48]. Here we extend this concept by characterising LRI310, a newly synthesised steroid-derived scaffold. In AlphaScreen assays, LRI310 inhibited the formation of the LIF, LIFR complex with submicromolar potency, confirming direct interference with ligand-receptor engagement. Computational docking and induced-fit simulations place LRI310 within the orthosteric cavity formed by the L1 loop of domain D3 and the L2-L3 loops of domain D4, a region previously shown to accommodate both LIF and other LIFR antagonists [20,38]. The predicted binding mode, stabilised by hydrophobic contacts and hydrogen bonds with W302 and A309, as well as interactions with V307, V311, T316, L331 and Y342, recapitulates the structural determinants identified for mifepristone and BAR502, but also highlights subtle conformational effects of the modified biphenyl moiety that may explain the lower potency of LRI310 compared with the parent compound 2o.

Functionally, LRI310 behaved LIFR antagonist in MIA-PaCa-2 cells. Co-treatment with LIF and LRI310 abrogated LIF-induced increases in cell viability, Ki-67 expression and cMYC transcription, reinstated G_0-G_1 arrest and enhanced apoptosis and counteracted EMT-like changes by reducing vimentin expression and fibre assembly and attenuated the acquisition of a migratory phenotype in wound-healing assays. In line with the central role of JAK/STAT3 downstream of LIFR [9], LRI310 dose-dependently suppressed LIF-stimulated STAT3 phosphorylation.

Pharmacological blockade of LIFR also disrupts the epithelial-stromal communication that underpins CAF activation. In a transwell co-culture system, we modelled the interaction between MIAPaCa-2 cells, representing the epithelial compartment, and human pancreatic stellate cells (HPanSteC), representing CAF precursors. Confocal imaging confirmed that HPanSteC are α-SMA^+ and LIFR-high but express minimal LIF, consistent with our human tissue observations. Under these conditions, epithelial exposure to LIF triggered a dual transcriptional response: in cancer cells, LIF re-induced inflammatory and interferon-related genes (CEBPD, IFI16, IFI30, BCL6) while repressing SNORA47, mirroring the monoculture RNA-seq signature; in stellate cells, conditioned signals from LIF-stimulated epithelium drove robust upregulation of *COL1A1, ACTA2, TGFB1* and *TIMP1*, indicative of a myofibroblastic, matrix-remodelling phenotype. Strikingly, LIFR blockade largely normalised these changes in both compartments, dampening epithelial inflammatory outputs and preventing fibroblast activation. These data provide functional evidence that the epithelial LIF program we identified is not merely a cell-intrinsic stress response but constitutes a paracrine mechanism that instructs stellate cells toward CAF fates, a process that can be pharmacologically intercepted by LIFR antagonists.

From a broader perspective, our findings fit within an emerging view of PDAC as a cytokine-driven ecosystem in which CAF heterogeneity is dynamically shaped by tumour-derived cues. Distinct CAF subsets have been shown to coexist and interconvert in response to gradients of TGF-β, IL-1, IL-6 family cytokines and interferons. By linking epithelial LIF to an integrated transcriptional program that encompasses IL-6/OSM signalling, NF-κB and interferon pathways, chemokines such as CCL5 and mechanotransductive effectors, our data suggest that LIF may act as a rheostat coordinating both inflammatory iCAF and contractile myCAF states. Importantly, the correlation of LIF with iCAF/myCAF signatures and with genes such as *CPXM1, C1QTNF3* and *CSRP2* in human PDAC reinforces the concept that LIF is not a redundant cytokine but a central organiser of stromal fitness.

In this context, LIFR antagonists like LRI310, mifepristone or BAR502 might provide a means to reprogramme the tumour microenvironment by simultaneously dampening epithelial aggressiveness and CAF-mediated desmoplasia.

In conclusion, this study identifies LIF as a potent epithelial driver of CAF-oriented transcriptional programs in PDAC and provides mechanistic and functional evidence that pharmacological antagonism of LIFR with the steroid-derived compound LRI310 can blunt these pro-tumorigenic signals. By integrating epithelial RNA-seq, patient-derived datasets, biochemical binding assays, structural modelling and co-culture systems, we delineate a coherent model in which LIF produced by cancer cells engages LIFR on both tumour and stromal compartments, amplifying inflammatory, profibrotic and migratory pathways that sustain PDAC progression.

Targeting this axis with small-molecule LIFR antagonists emerges as a promising strategy to concurrently restrain tumour cell fitness and remodel the desmoplastic stroma, with potential implications for combination therapies aimed at overcoming chemoresistance and immune exclusion in LIF-high PDAC.

CRediT authorship contribution statement

Cristina Di Giorgio: Writing – review & editing, Writing – original draft, Supervision, Project administration, Methodology, Investigation, Data curation. **Maria Rosaria Sette:** Formal analysis, Data curation. **Benedetta Sensini:** Formal analysis, Data curation. **Eleonora Giannelli:** Formal analysis, Data curation. **Ginevra Lachi:** Formal analysis, Data curation. **Silvia Marchianò:** Formal analysis, Data curation. **Francesca Paniconi:** Formal analysis, Data curation. **Carmen Massa:** Formal analysis, Data curation. **Ginevra Urbani:** Formal analysis, Data

curation. **Rosa De Gregorio:** Formal analysis, Data curation. **Valentina Sepe:** Writing – review & editing, Formal analysis. **Maria Chiara Monti:** Writing – review & editing, Formal analysis. **Federica Moraca:** Writing – original draft, Formal analysis, Data curation. **Bruno Catalanotti:** Writing – review & editing, Writing – original draft, Formal analysis, Data curation. **Fabio Cartaginese:** Methodology, Resources. **Eleonora Distrutti:** Writing – review & editing. **Angela Zampella:** Writing – review & editing. **Michele Biagioli:** Writing – review & editing. **Stefano Fiorucci:** Writing – review & editing, Validation, Supervision, Funding acquisition, Conceptualization.

Declaration of competing interest

The authors declare that they have no known competing financial interests or personal relationships that could have appeared to influence the work reported in this paper.

Data availability

Data will be made available on request.

References

[1] R.L. Siegel, K.D. Miller, A. Jemal, Cancer statistics, 2020, CA. Cancer J. Clin. 70 (2020) 7–30, https://doi.org/10.3322/caac.21590.

[2] M. Orth, P. Metzger, S. Gerum, J. Mayerle, G. Schneider, C. Belka, M. Schnurr, K. Lauber, Pancreatic ductal adenocarcinoma: biological hallmarks, current status, and future perspectives of combined modality treatment approaches, Radiat. Oncol. 14 (2019) 141, https://doi.org/10.1186/s13014-019-1345-6.

[3] K. Wright, T. Ly, M. Kriet, A. Czirok, S.M. Thomas, Cancer-associated fibroblasts: master tumor microenvironment modifiers, Cancers (Basel). 15 (2023), https://doi.org/10.3390/cancers15061899.

[4] A.D. Cox, S.W. Fesik, A.C. Kimmelman, J. Luo, C.J. Der, Drugging the undruggable RAS: mission possible? Nat. Rev. Drug Discov. 13 (2014) 828–851, https://doi.org/10.1038/nrd4389.

[5] T. Zhang, Y. Ren, P. Yang, J. Wang, H. Zhou, Cancer-associated fibroblasts in pancreatic ductal adenocarcinoma, Cell Death Dis. 13 (2022) 897, https://doi.org/10.1038/s41419-022-05351-1.

[6] Q. Sun, B. Zhang, Q. Hu, Y. Qin, W. Xu, W. Liu, X. Yu, J. Xu, The impact of cancer-associated fibroblasts on major hallmarks of pancreatic cancer, Theranostics 8 (2018) 5072–5087, https://doi.org/10.7150/thno.26546.

[7] E. Elyada, M. Bolisetty, P. Laise, W.F. Flynn, E.T. Courtois, R.A. Burkhart, J. A. Teinor, P. Belleau, G. Biffi, M.S. Lucito, S. Sivajothi, T.D. Armstrong, D.D. Engle, K.H. Yu, Y. Hao, C.L. Wolfgang, Y. Park, J. Preall, E.M. Jaffee, A. Califano, P. Robson, D.A. Tuveson, Cross-species single-cell analysis of pancreatic ductal adenocarcinoma reveals antigen-presenting cancer-associated fibroblasts, Cancer Discov. 9 (2019) 1102–1123, https://doi.org/10.1158/2159-8290.CD-19-0094.

[8] D. Öhlund, A. Handly-Santana, G. Biffi, E. Elyada, A.S. Almeida, M. Ponz-Sarvise, V. Corbo, T.E. Oni, S.A. Hearn, E.J. Lee, I.I.C. Chio, C.-I. Hwang, H. Tiriac, L. A. Baker, D.D. Engle, C. Feig, A. Kultti, M. Egeblad, D.T. Fearon, J.M. Crawford, H. Clevers, Y. Park, D.A. Tuveson, Distinct populations of inflammatory fibroblasts and myofibroblasts in pancreatic cancer, J. Exp. Med. 214 (2017) 579–596, https://doi.org/10.1084/jem.20162024.

[9] C. Di Giorgio, S. Marchianò, E. Marino, M. Biagioli, R. Roselli, M. Bordoni, R. Bellini, G. Urbani, A. Zampella, E. Distrutti, A. Donini, L. Graziosi, S. Fiorucci, Next-generation sequencing analysis of gastric cancer identifies the leukemia inhibitory factor receptor as a driving factor in gastric cancer progression and as a predictor of poor prognosis, Front. Oncol. 12 (2022) 939969, https://doi.org/10.3389/fonc.2022.939969.

[10] N.A. Nicola, J.J. Babon, Leukemia inhibitory factor (LIF), Cytokine Growth Factor Rev. 26 (2015) 533–544, https://doi.org/10.1016/j.cytogfr.2015.07.001.

[11] H. Kamohara, K. Sakamoto, T. Ishiko, S. Mita, Y. Masuda, T. Abe, M. Ogawa, Human carcinoma cell lines produce biologically active leukemia inhibitory factor (LIF), Res. Commun. Mol. Pathol. Pharmacol. 85 (1994) 131–140.

[12] S.A. Hunter, B.J. McIntosh, Y. Shi, R.A.P. Sperberg, C. Funatogawa, L. Labanieh, E. Soon, H.C. Wastyk, N. Mehta, C. Carter, T. Hunter, J.R. Cochran, An engineered ligand trap inhibits leukemia inhibitory factor as pancreatic cancer treatment strategy, Commun. Biol. 4 (2021) 452, https://doi.org/10.1038/s42003-021-01928-2.

[13] C. Di Giorgio, R. Bellini, A. Lupia, C. Massa, G. Urbani, M. Bordoni, S. Marchianò, R. Rosselli, R. De Gregorio, P. Rapacciuolo, V. Sepe, E. Morretta, M.C. Monti, F. Moraca, L. Cari, K.R.S. Ullah, N. Natalizi, L. Graziosi, E. Distrutti, M. Biagioli, B. Catalanotti, A. Donini, A. Zampella, S. Fiorucci, The leukemia inhibitory factor regulates fibroblast growth factor receptor 4 transcription in gastric cancer, Cell. Oncol. (Dordr) 47 (2023) 695–710, https://doi.org/10.1007/s13402-023-00893-8.

[14] S.M. Seifati, F. Zare, S.A.M. Bafghi, H. Hadinedoushan, Impact of anti leukemia inhibitory factor antibody on immune related gene expression in breast cancer Balb/c mouse model, Sci. Rep. 14 (2024) 20403, https://doi.org/10.1038/s41598-024-71014-0.

[15] R. De Gregorio, F. Moraca, P. Rapacciuolo, B. Fiorillo, E. Morretta, C. Di Giorgio, S. Marchianò, G. Lachi, C. Massa, B. Sensini, M. Biagioli, L. Spinelli, M.C. Monti, B. Catalanotti, V. Sepe, S. Fiorucci, A. Zampella, Harnessing the estradienone scaffold to develop dual GPBAR1 and LIFR modulators for liver fibrosis, J. Med. Chem. 68 (2025) 20037–20059, https://doi.org/10.1021/acs.jmedchem.5c00705.

[16] G.M. Sastry, M. Adzhigirey, T. Day, R. Annabhimoju, W. Sherman, Protein and ligand preparation: parameters, protocols, and influence on virtual screening enrichments, J. Comput. Aided Mol. Des. 27 (2013) 221–234, https://doi.org/10.1007/s10822-013-9644-8.

[17] J.C. Shelley, A. Cholleti, L.L. Frye, J.R. Greenwood, M.R. Timlin, M. Uchimaya, Epik: a software program for pK(a) prediction and protonation state generation for drug-like molecules, J. Comput. Aided Mol. Des. 21 (2007) 681–691, https://doi.org/10.1007/s10822-007-9133-z.

[18] J.L. Banks, H.S. Beard, Y. Cao, A.E. Cho, W. Damm, R. Farid, A.K. Felts, T. A. Halgren, D.T. Mainz, J.R. Maple, R. Murphy, D.M. Philipp, M.P. Repasky, L. Y. Zhang, B.J. Berne, R.A. Friesner, E. Gallicchio, R.M. Levy, Integrated modeling program, applied chemical theory (IMPACT), J. Comput. Chem. 26 (2005) 1752–1780, https://doi.org/10.1002/jcc.20292.

[19] L. Grippo, S. Lucidi, A globally convergent version of the Polak-Ribière conjugate gradient method, Math. Program. 78 (1997) 375–391, https://doi.org/10.1007/BF02614362.

[20] C. Di Giorgio, E. Morretta, A. Lupia, R. Bellini, C. Massa, G. Urbani, M. Bordoni, S. Marchianò, G. Lachi, P. Rapacciuolo, C. Finamore, V. Sepe, M. Chiara Monti, F. Moraca, N. Natalizi, L. Graziosi, E. Distrutti, M. Biagioli, B. Catalanotti, A. Donini, A. Zampella, S. Fiorucci, Bile acids serve as endogenous antagonists of the Leukemia inhibitory factor (LIF) receptor in oncogenesis, Biochem. Pharmacol. 223 (2024) 116134, https://doi.org/10.1016/j.bcp.2024.116134.

[21] P. Rapacciuolo, C. Finamore, C. Di Giorgio, B. Fiorillo, C. Massa, G. Urbani, S. Marchianò, M. Bordoni, C. Cassiano, E. Morretta, L. Spinelli, A. Lupia, F. Moraca, M. Biagioli, V. Sepe, M.C. Monti, B. Catalanotti, S. Fiorucci, A. Zampella, Design, synthesis, and pharmacological evaluation of dual FXR-LIFR modulators for the treatment of liver fibrosis, J. Med. Chem. 67 (2024) 18334–18355, https://doi.org/10.1021/acs.jmedchem.4c01651.

[22] 2025 Schrödinger Release 2025-1: Qm-Polarized Ligand Docking Protocol, Glide, Jaguar, Schrödinger, LLC QSite, Schrödinger; Schrödinger, LLC: New York, NY, ., (n.d.).

[23] 2021. Schrödinger Release 2023-1: Induced Fit Docking Protocol, Glide, Prime Schrödinger, LLC; Schrödinger, LLC: New York, NY, ., (n.d.).

[24] S. Viswanadhapalli, Y. Luo, G.R. Sareddy, B. Santhamma, M. Zhou, M. Li, S. Ma, R. Sonavane, U.P. Pratap, K.A. Altwegg, X. Li, A. Chang, A. Chávez-Riveros, K. V. Dileep, K.Y.J. Zhang, X. Pan, R. Murali, M. Bajda, G.V. Raj, A.J. Brenner, V. Manthati, M.K. Rao, R.R. Tekmal, H.B. Nair, K.J. Nickisch, R.K. Vadlamudi, EC359: a first-in-class small-molecule inhibitor for targeting oncogenic LIFR signaling in triple-negative breast cancer, Mol. Cancer Ther. 18 (2019) 1341–1354, https://doi.org/10.1158/1535-7163.MCT-18-1258.

[25] C.-Y. Ko, W.-C. Chang, J.-M. Wang, Biological roles of CCAAT/enhancer-binding protein delta during inflammation, J. Biomed. Sci. 22 (2015) 6, https://doi.org/10.1186/s12929-014-0110-2.

[26] S. Zimmermann, L. Pfannkuch, M.A. Al-Zeer, S. Bartfeld, M. Koch, J. Liu, C. Rechner, M. Soerensen, O. Sokolova, A. Zamyatina, P. Kosma, A.P. Mäurer, F. Glowinski, K.-P. Pleissner, M. Schmid, V. Brinkmann, A. Karlas, M. Naumann, M. Rother, N. Machuy, T.F. Meyer, ALPK1- and TIFA-dependent innate immune response triggered by the *Helicobacter pylori* type IV secretion system, Cell Rep. 20 (2017) 2384–2395, https://doi.org/10.1016/j.celrep.2017.08.039.

[27] X. Duan, L. Ponomareva, S. Veeranki, R. Panchanathan, E. Dickerson, D. Choubey, Differential roles for the interferon-inducible IFI16 and AIM2 innate immune sensors for cytosolic DNA in cellular senescence of human fibroblasts, Mol. Cancer Res. 9 (2011) 589–602, https://doi.org/10.1158/1541-7786.MCR-10-0565.

[28] C. Zhu, X. Chen, G. Guan, C. Zou, Q. Guo, P. Cheng, W. Cheng, A. Wu, IFI30 is a novel immune-related target with predicting value of prognosis and treatment response in glioblastoma, Onco. Targets. Ther. 13 (2020) 1129–1143, https://doi.org/10.2147/OTT.S237162.

[29] L.-F. Gao, Y. Zhong, T. Long, X. Wang, J.-X. Zhu, X.-Y. Wang, Z.-Y. Hu, Z.-G. Li, Tumor bud-derived CCL5 recruits fibroblasts and promotes colorectal cancer progression via CCR5-SLC25A24 signaling, J. Exp. Clin. Cancer Res. 41 (2022) 81, https://doi.org/10.1186/s13046-022-02300-w.

[30] Y.-H. Kim, J.L. Barclay, J. He, X. Luo, H.M. O'Neill, S. Keshvari, J.A. Webster, C. Ng, L.J. Hutley, J.B. Prins, J.P. Whitehead, Identification of carboxypeptidase X (CPX)-1 as a positive regulator of adipogenesis, FASEB J. Off. Publ. Fed. Am. Soc. Exp. Biol. 30 (2016) 2528–2540, https://doi.org/10.1096/fj.201500107R.

[31] A.C. Midgley, M. Rogers, M.B. Hallett, A. Clayton, T. Bowen, A.O. Phillips, R. Steadman, Transforming growth factor-β1 (TGF-β1)-stimulated fibroblast to myofibroblast differentiation is mediated by hyaluronan (HA)-facilitated epidermal growth factor receptor (EGFR) and CD44 co-localization in lipid rafts, J. Biol. Chem. 288 (2013) 14824–14838, https://doi.org/10.1074/jbc.M113.451336.

[32] N. Frangogiannis, Transforming growth factor-β in tissue fibrosis, J. Exp. Med. 217 (2020) e20190103, https://doi.org/10.1084/jem.20190103.

[33] C.-H. Chen, Y.-C. Ho, H.-H. Ho, I.-C. Chang, K.H. Kirsch, Y.-J. Chuang, M.D. Layne, S.-F. Yet, Cysteine-rich protein 2 alters p130Cas localization and inhibits vascular smooth muscle cell migration, Cardiovasc. Res. 100 (2013) 461–471, https://doi.org/10.1093/cvr/cvt207.

[34] D.-W. Wang, W.-H. Zhang, G. Danil, K. Yang, J.-K. Hu, The role and mechanism of claudins in cancer, Front. Oncol. 12 (2022) 1051497, https://doi.org/10.3389/fonc.2022.1051497.

[35] G.S. Bogatkevich, E. Gustilo, J.C. Oates, C. Feghali-Bostwick, R.A. Harley, R. M. Silver, A. Ludwicka-Bradley, Distinct PKC isoforms mediate cell survival and DNA synthesis in thrombin-induced myofibroblasts, Am. J. Physiol. Cell. Mol. Physiol. 288 (2005) L190–L201, https://doi.org/10.1152/ajplung.00448.2003.
[36] D.-Y. Chen, N.-H. Sun, X. Chen, J.-J. Gong, S.-T. Yuan, Z.-Z. Hu, N.-N. Lu, J. Körbelin, K. Fukunaga, Q.-H. Liu, Y.-M. Lu, F. Han, Endothelium-derived semaphorin 3G attenuates ischemic retinopathy by coordinating β-catenin-dependent vascular remodeling, J. Clin. Invest. 131 (2021), https://doi.org/10.1172/JCI135296.
[37] J.E. Kolodsick, M. Peters-Golden, J. Larios, G.B. Toews, V.J. Thannickal, B. B. Moore, Prostaglandin E2 inhibits fibroblast to myofibroblast transition via *E. prostanoid* receptor 2 signaling and cyclic adenosine monophosphate elevation, Am. J. Respir. Cell Mol. Biol. 29 (2003) 537–544, https://doi.org/10.1165/rcmb.2002-0243OC.
[38] C. Di Giorgio, A. Lupia, S. Marchianò, M. Bordoni, R. Bellini, C. Massa, G. Urbani, R. Roselli, F. Moraca, V. Sepe, B. Catalanotti, E. Morretta, M.C. Monti, M. Biagioli, E. Distrutti, A. Zampella, S. Fiorucci, Repositioning mifepristone as a leukaemia inhibitory factor receptor antagonist for the treatment of pancreatic adenocarcinoma, Cells 11 (2022) 3482, https://doi.org/10.3390/cells11213482.
[39] T. Huyton, J.-G. Zhang, C.S. Luo, M.-Z. Lou, D.J. Hilton, N.A. Nicola, T.P.J. Garrett, An unusual cytokine:Ig-domain interaction revealed in the crystal structure of leukemia inhibitory factor (LIF) in complex with the LIF receptor, Proc. Natl. Acad. Sci. 104 (2007) 12737–12742, https://doi.org/10.1073/pnas.0705577104.
[40] T. Nagasaki, M. Hara, H. Nakanishi, H. Takahashi, M. Sato, H. Takeyama, Interleukin-6 released by colon cancer-associated fibroblasts is critical for tumour angiogenesis: anti-interleukin-6 receptor antibody suppressed angiogenesis and inhibited tumour-stroma interaction, Br. J. Cancer 110 (2014) 469–478, https://doi.org/10.1038/bjc.2013.748.
[41] O.E. Franco, M. Jiang, D.W. Strand, J. Peacock, S. Fernandez, R.S. Jackson 2nd, M. P. Revelo, N.A. Bhowmick, S.W. Hayward, Altered TGF-β signaling in a subpopulation of human stromal cells promotes prostatic carcinogenesis, Cancer Res. 71 (2011) 1272–1281, https://doi.org/10.1158/0008-5472.CAN-10-3142.
[42] R. Kalluri, M. Zeisberg, Fibroblasts in cancer, Nat. Rev. Cancer 6 (2006) 392–401, https://doi.org/10.1038/nrc1877.
[43] K. Wang, F. Wu, B.R. Seo, C. Fischbach, W. Chen, L. Hsu, D. Gourdon, Breast cancer cells alter the dynamics of stromal fibronectin-collagen interactions, Matrix Biol. 60–61 (2017) 86–95, https://doi.org/10.1016/j.matbio.2016.08.001.
[44] N. Vaziri, L. Shariati, A. Zarrabi, A. Farazmand, S. Haghjooy Javanmard, Cancer-associated fibroblasts regulate the plasticity of breast cancer stemness through the production of Leukemia inhibitory factor, Life (Basel, Switzerland) 11 (2021), https://doi.org/10.3390/life11121298.
[45] F. Peng, J. Zhou, W. Sheng, D. Zhang, M. Dong, Expression and significance of leukemia inhibitory factor in human pancreatic cancer, Zhonghua Yi Xue Za Zhi 94 (2014) 90–95.
[46] M. Pascual-García, E. Bonfill-Teixidor, E. Planas-Rigol, C. Rubio-Perez, R. Iurlaro, A. Arias, I. Cuartas, A. Sala-Hojman, L. Escudero, F. Martínez-Ricarte, I. Huber-Ruano, P. Nuciforo, L. Pedrosa, C. Marques, I. Braña, E. Garralda, M. Vieito, M. Squatrito, E. Pineda, F. Graus, C. Espejo, J. Sahuquillo, J. Tabernero, J. Seoane, LIF regulates CXCL9 in tumor-associated macrophages and prevents CD8(+) T cell tumor-infiltration impairing anti-PD1 therapy, Nat. Commun. 10 (2019) 2416, https://doi.org/10.1038/s41467-019-10369-9.
[47] G.K. Arora, A. Gupta, S. Narayanan, T. Guo, P. Iyengar, R.E. Infante, Cachexia-associated adipose loss induced by tumor-secreted leukemia inhibitory factor is counterbalanced by decreased leptin, JCI Insight 3 (2018), https://doi.org/10.1172/jci.insight.121221.
[48] C. Di Giorgio, R. Bellini, A. Lupia, C. Massa, M. Bordoni, S. Marchianò, R. Rosselli, V. Sepe, P. Rapacciuolo, F. Moraca, E. Morretta, P. Ricci, G. Urbani, M.C. Monti, M. Biagioli, E. Distrutti, B. Catalanotti, A. Zampella, S. Fiorucci, C. Di Giorgio, R. Bellini, A. Lupia, C. Massa, M. Bordoni, S. Marchianò, R. Rosselli, V. Sepe, P. Rapacciuolo, F. Moraca, E. Morretta, P. Ricci, G. Urbani, M.C. Monti, M. Biagioli, E. Distrutti, B. Catalanotti, A. Zampella, S. Fiorucci, Discovery of BAR502, as potent steroidal antagonist of leukemia inhibitory factor receptor for the treatment of pancreatic adenocarcinoma, Front. Oncol. 13 (2023) 1140730, https://doi.org/10.3389/fonc.2023.1140730.